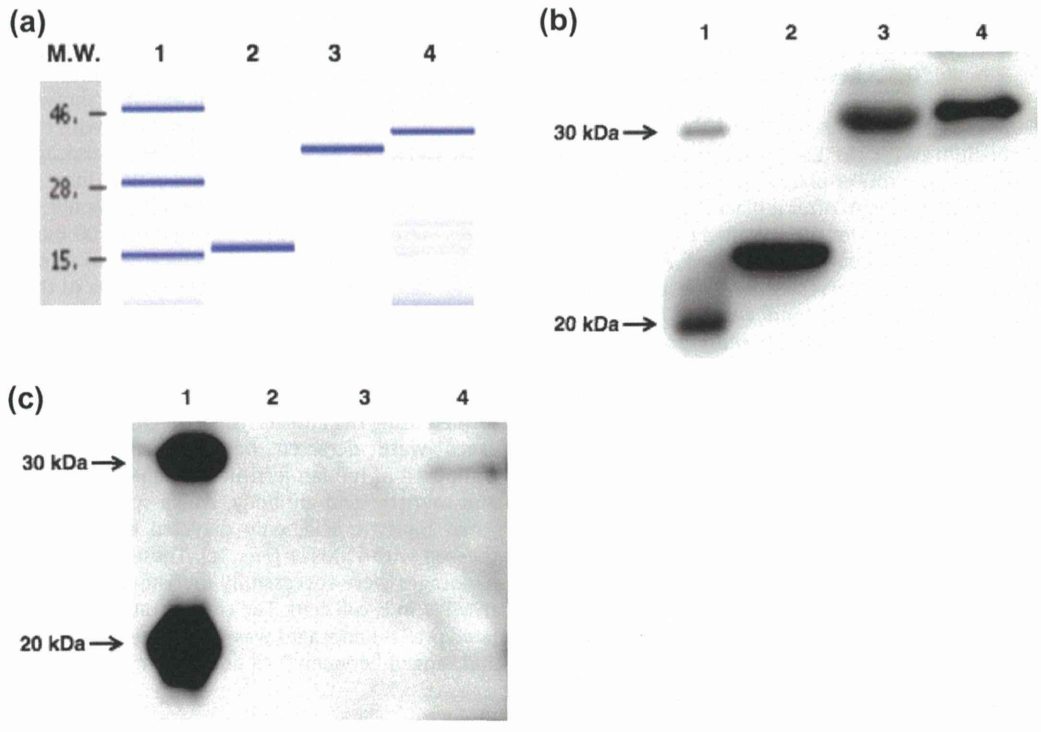

Fig. 3. SDS–PAGE and Western blot analyses of the engineered nanocages. (a) Chip gel images. Lane 1, molecular mass ladder (15, 28, and 46 kDa); lane 2, control nanocage (rh-ferritin-L); lanes 3 and 4, preS1–nanocage without or with co-expressed rNMT-1. (b, c) Western blot analyses of purified nanocages using anti-ferritin light chain (b) and anti-myristic acid (conjugated) (c) antibodies. lane 1, MagicMark XP Western protein standard (Life Technologies); lane 2, control nanocage (rh-ferritin-L); lanes 3 and 4, preS1–nanocage without or with co-expressed rNMT-1.

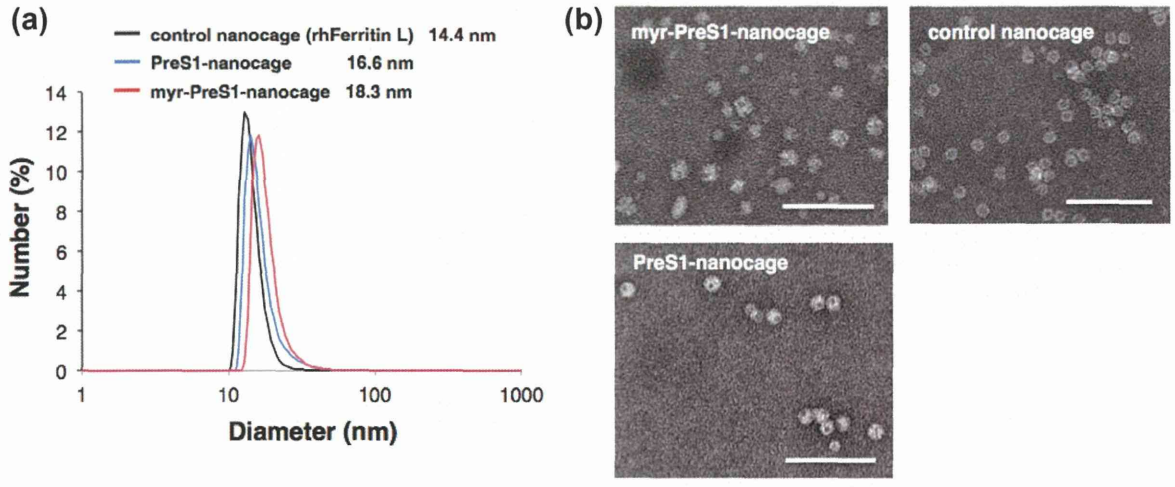

Fig. 4. Size and shape distribution of the nanocage determined by DLS (a) and TEM (b). The numbers in (a) are the mean hydrodynamic diameters of the DLS distribution. The protein nanocages were stained with 2% uranyl acetate for TEM. Scale bar = 100 nm.

Targeted delivery of myristoylated preS1–nanocages to hepatocyte-like cells

Because cell cytotoxicity is an important factor in the selection of materials for drug carriers, the nanocages produced here were characterized regarding their effects on cell viability in the same conditions used in the fluorescence assay of cellular uptake experiments. The preS1–nanocages and the myristoylated preS1–nanocages did not have any appreciable cytotoxic effects under these conditions (Fig. S3). Similar results were obtained using control nanocages under the same conditions (data not shown). For cellular uptake experiments using quantitative flow cytometry analysis, fluorophore-labeled nanocages were prepared using Alexa Fluor® 488 succinimidyl ester. Successful modification with the fluorophore was confirmed by SDS–PAGE (data not shown). We next performed transfection assays to determine whether fusion of the preS1 peptide into the ferritin-L nanocage enhanced the binding affinity of the nanocage towards human hepatoma HepaRG cells, the specific target cells of myristoylated preS1 peptide. HepaRG cell-associated fluorescence was significantly increased after incubation with the Alexa Fluor 488-labeled, myristoylated preS1–nanocages (Fig. 5). The geometric mean

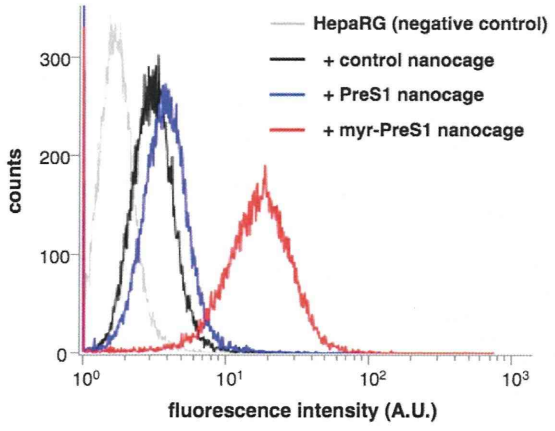

Fig. 5. Representative histograms of the fluorescence intensities of HepaRG cells incubated with fluorophore-labeled nanocages in the presence of 10% fetal bovine serum.

fluorescence intensity clearly confirmed that the myristoylated preS1–nanocages bound to hepatoma cells *in vitro*. Although the HepaRG cells exhibit a background level of autofluorescence, the geometric mean fluorescence intensity was negligible. By contrast, flow cytometric analysis showed that the nonspecific binding of Alexa Fluor 488-labeled control nanocages and unmyristoylated preS1–nanocages to HepaRG cells was very low. These results clearly indicate that myristoylation of the nanocages is important for mediating the cellular entry of the nanocages. It is often considered that acylation has several roles, including promoting the interaction between proteins and hydrophobic membranes, and anchoring acylated proteins to the cytoplasmic side of the lipid bilayer [1,3]. However, many myristoylated proteins are localized to the cytoplasm and the myristoyl moiety seems to mediate protein–protein interactions rather than simple protein–membrane lipid interactions [18–20]. Indeed, HBV-derived synthetic preS1–lipopeptides inhibit specific HBV receptor–ligand interactions on hepatic cells [21]. The myristoylated preS1–nanocages seem to target hepatocyte-like cells through a similar mechanism.

In conclusion, we have described a simple method for lipid modification of protein nanocages using a co-expression system in *E. coli*. This modification improved the specificity of these nanocages towards target cells. To the best of our knowledge, this is the first report describing the myristoylation of such a huge protein complex. In the future, we intend to examine the *in vivo* properties of these myristoylated preS1–nanocages as a new drug delivery system.

Acknowledgments

This work was supported by a Health Labour Sciences Research Grant (Research on Publicly Essential Drugs and Medical Devices) from the Ministry of Health, Labour and Welfare of Japan. M. Murata was partially supported by Special Coordination Funds for Promoting Science and Technology of Japan (Siouxland Community Foundation funding program "Innovation Center for Medical Redox Navigation"); and a Grant-in-Aid for Scientific Research (Nos. 25560225 and 24300172) from the Ministry of Education, Culture, Sports, Science, and Technology of Japan (MEXT).

Appendix A. Supplementary data

Supplementary data associated with this article can be found, in the online version, at http://dx.doi.org/10.1016/j.pep.2014.12.001.

References

[1] C.T. Walsh, S. Garneau-Tsodikova, G.J. Gatto Jr., Protein posttranslational modifications: the chemistry of proteome diversifications, Angew. Chem. Int. Ed. 44 (2005) 7342–7372.
[2] R.N. Hannoush, J. Sun, The chemical toolbox for monitoring protein fatty acylation and prenylation, Nat. Chem. Biol. 6 (2010) 498–506.
[3] M.D. Resh, Trafficking and signaling by fatty-acylated and prenylated proteins, Nat. Chem. Biol. 2 (2006) 584–590.
[4] K. Sao, M. Murata, Y. Fujisaki, K. Umezaki, T. Mori, T. Niidome, Y. Katayama, M. Hashizume, A novel protease activity assay using a protease-responsive chaperone protein, Biochem. Biophys. Res. Commun. 383 (2009) 293–297.
[5] K. Sao, M. Murata, K. Umezaki, Y. Fujisaki, T. Mori, T. Niidome, Y. Katayama, M. Hashizume, Molecular design of protein-based nanocapsules for stimulus-responsive characteristics, Biorg. Med. Chem. 17 (2009) 85–93.
[6] M. Murata, S. Narahara, K. Umezaki, R. Toita, S. Tabata, J.S. Piao, K. Abe, J.H. Kang, K. Ohuchida, L. Cui, M. Hashizume, Liver cell specific targeting by the preS1 domain of hepatitis B virus surface antigen displayed on protein nanocages, Int. J. Nanomed. 7 (2012) 4353–4362.
[7] R. Toita, M. Murata, S. Tabata, K. Abe, S. Narahara, J.S. Piao, J.H. Kang, M. Hashizume, Development of human hepatocellular carcinoma cell-targeted protein cages, Bioconjug. Chem. 23 (2012) 1494–1501.
[8] R. Toita, M. Murata, K. Abe, S. Narahara, J.S. Piao, J.H. Kang, M. Hashizume, A nanocarrier based on a genetically engineered protein cage to deliver doxorubicin to human hepatocellular carcinoma cells, Chem. Commun. 49 (2013) 7442–7444.
[9] R. Toita, M. Murata, K. Abe, S. Narahara, J.S. Piao, J.H. Kang, K. Ohuchida, M. Hashizume, Biological evaluation of protein nanocapsules containing doxorubicin, Int. J. Nanomed. 8 (2013) 1989–1999.
[10] J.H. Kang, R. Toita, D. Asai, T. Yamaoka, M. Murata, Liver cell-specific peptides derived from the preS1 domain of human hepatitis B virus, J. Virol. Methods 201 (2014) 20–23.
[11] Y.J. Yang, P.S. Zhao, H.X. Wu, H.L. Wang, L.L. Zhao, X.H. Xue, W.W. Gai, Y.W. Gao, S.T. Yang, X.Z. Xia, Production and characterization of a fusion peptide derived from the rabies virus glycoprotein (RVG29), Protein Expr. Purif. 104C (2014) 7–13.
[12] X. Zhao, Y. Dong, Z. Zhao, J. Guo, J. Liu, P. Huang, D. Dong, H. Fan, Q. Guo, X. Yang, J. Xu, J. Li, L. Fu, W. Chen, Intracellular delivery of artificial transcription factors fused to the protein transduction domain of HIV-1 Tat, Protein Expr. Purif. 90 (2013) 27–33.
[13] J. Jung, M. Iijima, N. Yoshimoto, M. Sasaki, T. Niimi, K. Tatematsu, S.Y. Jeong, E.K. Choi, K. Tanizawa, S. Kuroda, Efficient and rapid purification of drug- and gene-carrying bio-nanocapsules, hepatitis B virus surface antigen L particles, from *Saccharomyces cerevisiae*, Protein Expr. Purif. 78 (2011) 149–155.
[14] D. Glebe, S. Urban, E.V. Knoop, N. Çağ, P. Krass, S. Grün, A. Bulavaite, K. Sasnauskas, W.H. Gerlich, Mapping of the hepatitis B virus attachment site by use of infection-inhibiting preS1 lipopeptides and tupaia hepatocytes, Gastroenterology 129 (2005) 234–245.
[15] T. Muller, S. Mehrle, A. Schieck, U. Haberkorn, S. Urban, W. Mier, Liver imaging with a novel hepatitis B surface protein derived SPECT-tracer, Mol. Pharm. 10 (2013) 2230–2236.
[16] K. Hintze, E. Theil, Cellular regulation and molecular interactions of the ferritins, Cell. Mol. Life Sci. 63 (2006) 591–600.
[17] Z. Wang, C. Li, M. Ellenburg, E. Soistman, J. Ruble, B. Wright, J.X. Ho, D.C. Carter, Structure of human ferritin L chain, Acta Crystallogr. D Biol. Crystallogr. 62 (2006) 800–806.
[18] S. Maurer-Stroh, F. Eisenhaber, Myristoylation of viral and bacterial proteins, Trends Microbiol. 12 (2004) 178–185.
[19] D.D. Martin, E. Beauchamp, L.G. Berthiaume, Post-translational myristoylation: fat matters in cellular life and death, Biochimie 93 (2011) 18–31.
[20] A. Arzumanyan, H.M. Reis, M.A. Feitelson, Pathogenic mechanisms in HBV- and HCV-associated hepatocellular carcinoma, Nat. Rev. Cancer 13 (2013) 123–135.
[21] A. Meier, S. Mehrle, T.S. Weiss, W. Mier, S. Urban, Myristoylated preS1-domain of the hepatitis B virus L-protein mediates specific binding to differentiated hepatocytes, Hepatology 58 (2013) 31–42.

Supporting Information

Control nanocage (rh-ferritin-L) (175 amino acids, molecular weight = 19 986 Da)
MSSQIRQNYSTDVEAAVNSLVNLYLQASYTYLSLGFYFDRDDVALEGVSHFFREL
AEEKREGYERLLKMQNQRGGRALLQDIKKPAEDEWGKTPDAMKAAMALEKKLN
QALLDLHALGSARTDPHLCDFLETHFLDEEVKLIKKMGDHLTNLHRLGGPEAGLG
EYLFERLTLKHD

PreS1–nanocage (270 amino acids, molecular weight = 29 690 Da)
MGGWSSKPRKGMGTNLSVPNPLGFFPDHQLDPAFRANSNNPDWDFNPPDDDDKT
SGGSGGESEGESEGESEGESEGESEGESEGESEGESEGSPSGSSQIRQNYSTDVEAA
VNSLVNLYLQASYTYLSLGFYFDRDDVALEGVSHFFRELAEEKREGYERLLKMQN
QRGGRALLQDIKKPAEDEWGKTPDAMKAAMALEKKLNQALLDLHALGSARTDP
HLCDFLETHFLDEEVKLIKKMGDHLTNLHRLGGPEAGLGEYLFERLTLKHD

rNMT-1 (456 amino acids, molecular weight = 52 896 Da)
MGSEEDKAKKLENLLKLLQLNNDDTSKFTQEQKKAMKDHKFWRTQPVKDFDEK
VVEEGPIDKPKTPEDISDKPLPLLSSFEWCSIDVDNKKQLEDVFVLLNENYVEDRD
AGFRFNYTKEFFNWALKSPGWKKDWHIGVRVKETQKLVAFISAIPVTLGVRGKQ
VPSVEINFLCVHKQLRSKRLTPVLIKEITRRVNKCDIWHALYTAGIVLPAPVSTCRY
THRPLNWKKLYEVDFTGLPDGHTEEDMIAENALPAKTKTAGLRKLKKEDIDQVFE
LFKRYQSRFELIQIFTKEEFEHNFIGEESLPLDKQVIFSYVVEQPDGKITDFFSFYSLP
FTILNNTKYKDLGIGYLYYYATDADFQFKDRFDPKATKALKTRLCELIYDACILAK
NANMDVFNALTSQDNTLFLDDLKFGPGDGFLNFYLFNYRAKPITGGLNPDNSNDI
KRRSNVGVVML

Fig. S1. Amino acid sequences of the engineered nanocages. The preS1 peptide and the linker moiety are indicated by gray shading and underlining, respectively.

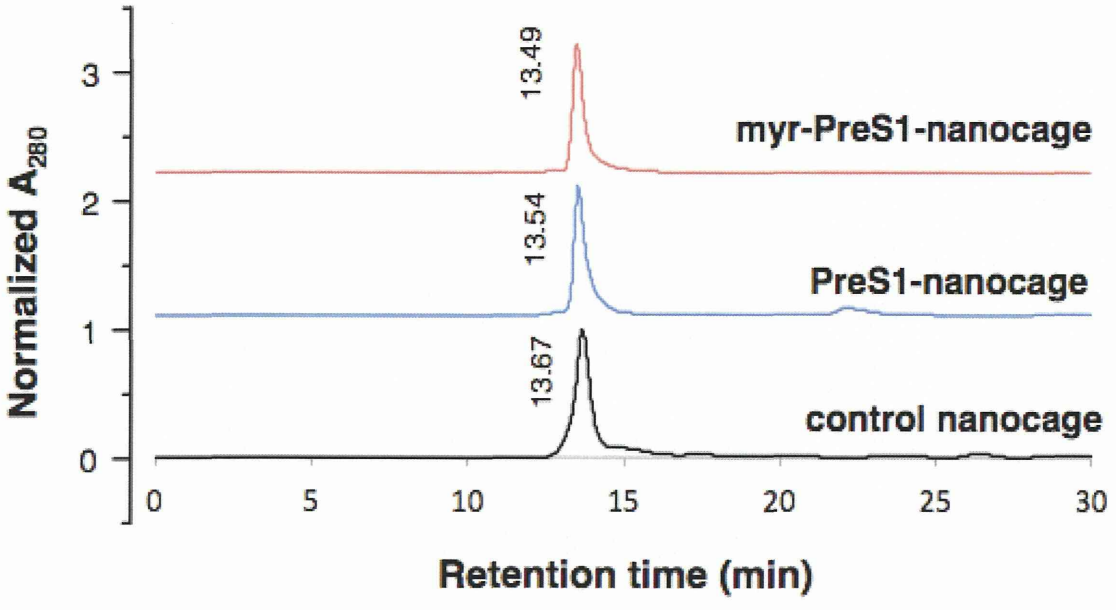

Fig. S2. Size exclusion chromatography of the nanocages.

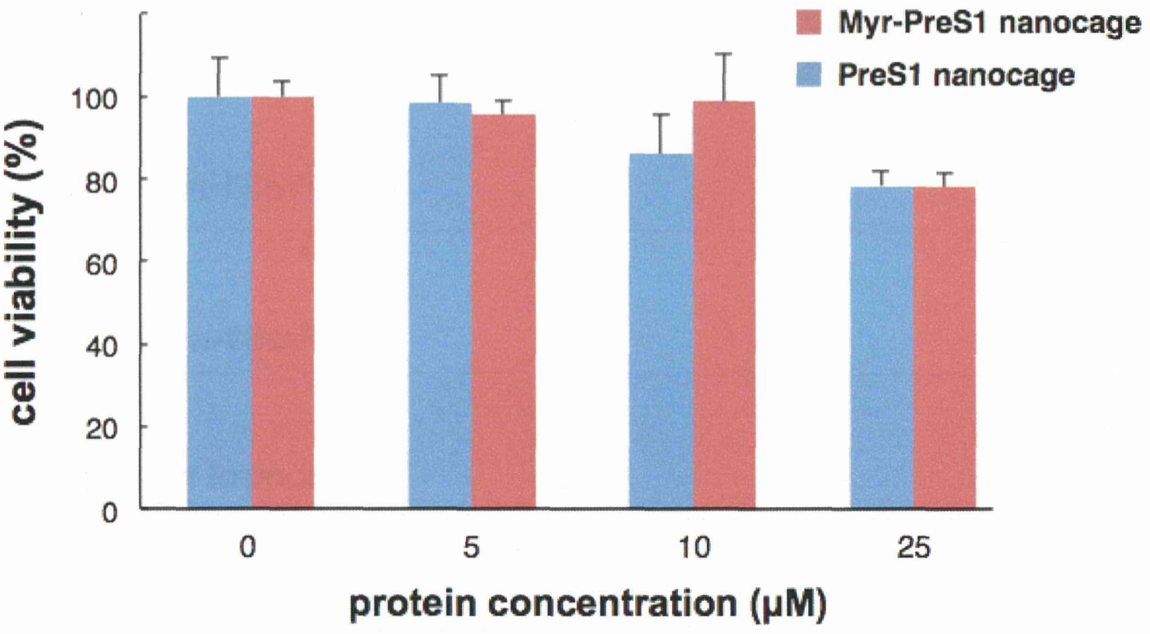

Fig. S3. Viability of HepaRG cells treated with preS1–nanocages and myristoylated preS1–nanocages. Cells were harvested on white-bottomed 96-well plates at an initial cell density of 10 000 cells/well, and were grown overnight. Then, 100 μl of nanocages dissolved in Dulbecco's modified Eagle's medium (1–25 μM) was added to each well and incubated for 48 h. Cell viability was measured using a CellTiter-Glo® luminescent cell viability assay kit (Promega, Madison, WI, USA). Luminescent intensity was measured using an ARVO MX 1420 microplate reader (PerkinElmer, Waltham, MA, USA).

Bioconjugate Chemistry

Communication

pubs.acs.org/bc

Fluorescent Polyion Complex Nanoparticle That Incorporates an Internal Standard for Quantitative Analysis of Protein Kinase Activity

Takanobu Nobori,[†] Shujiro Shiosaki,[‡] Takeshi Mori,[†,‡,§] Riki Toita,[‡] Chan Woo Kim,[‡] Yuta Nakamura,[‡] Akihiro Kishimura,[†,‡,∥] Takuro Niidome,[¶] and Yoshiki Katayama*[,†,‡,§,∥,⊥,#]

[†]Department of Applied Chemistry, Faculty of Engineering, [‡]Graduate School of Systems Life Sciences, [§]Center for Future Chemistry, [∥]International Research Center for Molecular Systems, [⊥]Center for Advanced Medical Innovation, and [#]Innovation Center for Medical Redox Navigation, Kyushu University, 744 Motooka, Nishi-ku, Fukuoka 819-0395, Japan

[¶]Graduate School of Science and Technology, Kumamoto University, 2-39-1 Kurokami, Chuo-Ku, Kumamoto 860-8555, Japan

Supporting Information

ABSTRACT: We demonstrate a polyion complex (PIC) nanoparticle that contains both a responsive fluorophore and an "internal standard" fluorophore for quantitative measurement of protein kinase (PK) activity. The PK-responsive fluorophore becomes more fluorescent with PK-catalyzed phosphorylation of substrate peptides incorporated in the PIC, while fluorescence from the internal standard remains unchanged during phosphorylation. This new concept will be useful for quantitative PK assays and the discovery of PK inhibitors.

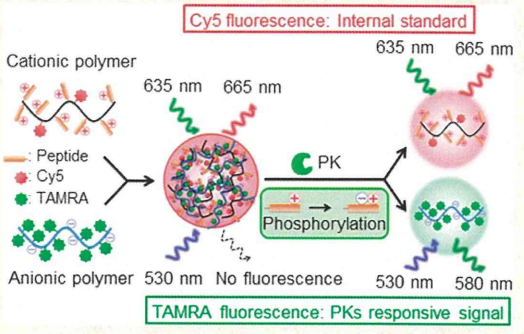

INTRODUCTION

Protein kinase (PK)-mediated phosphorylation plays a pivotal role in the regulation of cellular processes, and its dysfunction results in various human diseases, notably cancer.[1] Thus, PKs are primary molecular targets for anticancer drugs,[2] and tracking PK activity would be valuable for understanding molecular mechanisms of complex cellular events and subsequent drug development.[3] Measurement of PK activity via fluorescent readout is an attractive alternative to radioactive isotopes.[4−7] Several measurement kits for fluorescence-based PK activity such as LanthaScreen and Z′-LYTE are now commercially available and they are basically end-point assay. To realize real-time kinetic analysis and monitoring of activity in living cells, the fluorescent probes which "turn on" during phosphorylation of substrate peptides by the PKs have been proposed. The turn-on-type probes provide relatively sharp contrast in simple optical readout systems.[8,9] Mechanisms for these fluorescence responses to phosphorylation include metal complex formation,[10−15] protein recognition,[16−19] and concentration quenching.[20,21]

However, quantitative evaluation of PK activity is difficult for probes that turn on, especially for intracellular PKs, because the fluorescence signals depend not only on the PK activity, but also on the probe concentration. This is why fluorescence resonance energy transfer (FRET) is powerful, because it enables quantitative analysis via ratiometric fluorimetry.[5,22,23] However, FRET probes require strict molecular design, and repeated trial and error, to realize dynamic and appropriate distance changes upon phosphorylation.[24,25]

Here, we demonstrate a novel method to quantitatively measure PK activity that is based on a polymeric nanoparticle embedded with both a PK-responsive fluorophore and another fluorophore that is used as an internal standard for quantitative analysis of the PK activity. As shown in Figure 1a, the particle is a polyion complex (PIC) of cationic and anionic polymers. The cationic polymer is a neutral dextran main chain modified with both a cationic peptide substrate for PK and a Cy5 fluorophore (Figure 1b), while the anionic polymer is an anionic poly(L-aspartic acid) main chain modified with tetramethylrhodamine (TAMRA) (Figure 1c). In the PIC, the TAMRA fluorescence is selectively quenched, while the constant Cy5 fluorescence acts as the internal standard. This behavior is achieved by having a high enough concentration of TAMRA in the PIC to induce concentration quenching, and a low enough concentration of Cy5 to avoid it. When the cationic peptides in the cationic polymer are phosphorylated by a target PK, the negatively charged phosphate groups weaken or dissociate the PICs, which in turn reduces the TAMRA concentration quenching and allows more fluorescence. By remaining constant, the Cy5 fluorescence essentially normalizes the TAMRA signal. We demonstrate how the PIC can be used to detect protein kinase Cα (PKCα) activity, which is regarded as an important target for anticancer drugs because it is involved in cancer proliferation signaling.[26,27] Thus, a PKCα-specific substrate

Received: April 1, 2014
Revised: April 29, 2014
Published: May 2, 2014

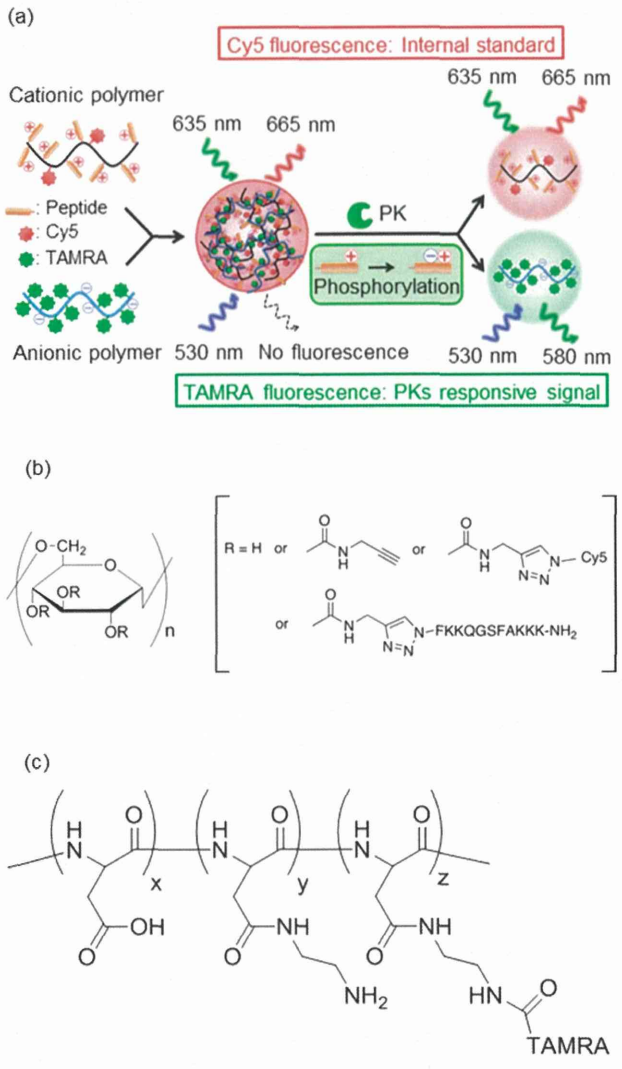

Figure 1. Schematic of a turn-on fluorescent probe, with an internal standard, for quantitative measurement of PK activity (a). Structures of cationic (b) and anionic (c) polymers.

peptide was used here (-FKKQGSFAKKK-NH_2), which changes its net cationic charge from +5 to +3 upon phosphorylation.

■ RESULTS AND DISCUSSION

The cationic and anionic polymers were synthesized to achieve uneven quenching behavior of the two fluorophores as depicted in Figure 1a. According to our previous report, a high fluorophore content in the polymers does not work for quench-to-recovery-type measurements because the fluorescence can be quenched by hydrophobic intramolecular association among the fluorophores prior to PIC formation.[28] Previously, we found that a few mol % of TAMRA had the best performance;[28] thus, the TAMRA content in the anionic polymer was adjusted to 2.1 mol %. In contrast, the content of Cy5 had to be small enough to avoid concentration quenching in the PIC, but large enough to provide a strong internal standard. In the previous research, we also found that a lower content of a fluorophore (<1.1 mol %) effectively avoids the quenching.[28] Thus, the content of Cy5 in the cationic polymer was lowered to be 0.4 mol %. Meanwhile, the content of the cationic peptide was adjusted to be relatively high (7.8 mol %) to achieve tight PIC formation. The cationic peptide and Cy5 were quantitatively introduced onto the dextran main chain by using "click chemistry".

We compared the reactivity of the substrate peptide that was grafted onto the cationic polymer with a free peptide by using a coupled enzyme assay,[29,30] in which phosphorylation by PK is estimated by absorbance at 340 nm. As shown in Figure 2, the

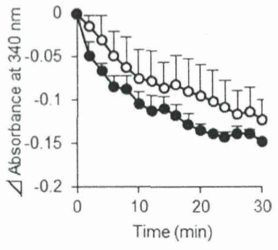

Figure 2. Comparison of the reactivity toward PKCα of free peptides (open circles) and peptides grafted onto the cationic polymer (closed circles). Peptide concentration in both cases is 30 μM; PKCα concentration is 1 U/mL.

substrate peptides on the cationic polymer exhibited almost identical reactivity toward PKCα as that for free peptides, indicating that the effect of substrate immobilization is negligible.

First, we evaluated concentration quenching of TAMRA in the anionic polymer by PIC formation, and avoided Cy5 quenching in the cationic polymer. Figure 3a shows

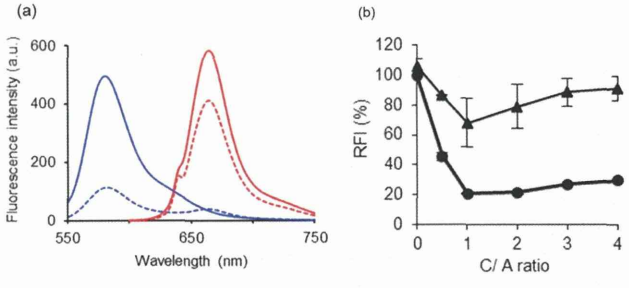

Figure 3. (a) Fluorescence spectra of Cy5 in the cationic polymer and in the PIC (red solid and broken lines, respectively, Ex. at 635 nm), and TAMRA in the anionic polymer and in the PIC (blue solid and broken lines, respectively, Ex. at 530 nm). The C/A ratio was 2. (b) Uneven quenching behavior of TAMRA (closed circles) and Cy5 fluorescence (closed triangles) in PIC prepared with varying C/A ratios. RFI is the relative fluorescence intensity of TAMRA and Cy5. Ex/Em of TAMRA and Cy5 was 530/590 and 635/665, respectively.

fluorescence spectra of the cationic and anionic polymers and the PIC prepared at a cation/anion (C/A) ratio of 2. TAMRA fluorescence in the anionic polymer was quenched to 20% of its original level by PIC formation, while the Cy5 fluorescence intensity was maintained at a high level (>70%). Thus, quenching of each fluorophore can be independently controlled by adjusting its density.

Figure 3b plots the fluorescence of TAMRA and Cy5 as a function of C/A ratios. TAMRA quenching leveled off at 20% at C/A = 1, while Cy5 fluorescence remained at about 70–80%, above C/A = 2. Both TAMRA and Cy5 fluorescence are minimized at C/A = 1, and both slightly increase with C/A > 1. This can be explained by the relaxation of the PIC from the

dx.doi.org/10.1021/bc500142j | Bioconjugate Chem. 2014, 25, 869–872

electrostatic repulsion caused by overcharging at higher C/A.[31] Hereafter we used PIC prepared at the C/A ratio of 2 for monitoring of PK activity. The size of the PIC at this C/A ratio was determined by dynamic light scattering to be 140 ± 2.3 nm (polydispersity index: 0.32).

Figure 4a,b plots the time dependences of TAMRA and Cy5 fluorescence, respectively, following the addition of various

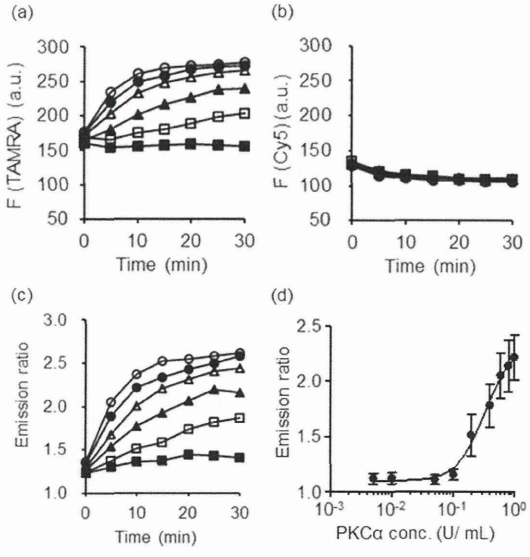

Figure 4. Time dependence of TAMRA (a) and Cy5 (b) fluorescence from PICs triggered by phosphorylation of the substrate peptide grafted onto the cationic polymers at various PKCα concentrations (■ 0, □ 0.2, ▲ 0.4, △ 0.6, ● 0.8, ○ 1.0 U/mL). (c) TAMRA/Cy5 emission ratio calculated from (a) and (b). (d) PKCα concentration dependence of the emission ratio after 30 min of phosphorylation.

concentrations of PKCα (0−1.0 U/mL) to the PIC dispersion. The TAMRA fluorescence increased rapidly with increasing PKCα concentration because of the weakened PICs. Meanwhile, the Cy5 fluorescence was almost constant over the same time span irrespective of PKCα concentration. These results clearly show that Cy5 fluorescence can be used as the internal standard to monitor the PKCα activity using the turning-on fluorescence of TAMRA. Thus, TAMRA fluorescence was normalized by Cy5 fluorescence and the normalized values (TAMRA/Cy5 emission ratio) are plotted in Figure 4c. At the highest PKCα concentration (1.0 U/mL), the ratio levels off at 2.5 after 15 min. Figure 4d plots the PKCα concentration dependence of the ratio at 30 min from the start of the phosphorylation. From this curve, the EC_{50} (50% effective concentration) of PKCα was calculated and found to be 0.34 U/mL, and the detection limit of PKCα was determined to be 0.29 U/mL (=182 ng/mL), which is comparable or more sensitive than that for other PK assays.[9,28,32]

Finally, we demonstrated determination of the IC_{50} (half maximal inhibitory concentration) of PKCα inhibitors using the PIC probe. Here we used two kinds of PKCα inhibitors, Gö6983 and Ro-31-8425, which have similar IC_{50} values; 7 nM for Gö6983[33] and 8 nM for Ro-31-8425.[34] Phosphorylation of PICs by 0.6 U/mL PKCα was performed for 30 min in the presence of the inhibitors at various concentrations. After the reactions, the TAMRA and Cy5 fluorescence intensities were measured to calculate the emission ratio, with Cy5 fluorescence being the internal standard. As shown in Figure 5a and b, the

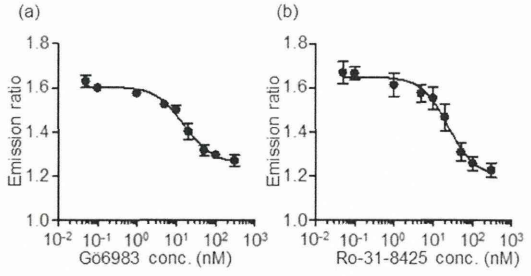

Figure 5. Inhibition of PKCα activity by specific inhibitors, Gö6983 (a) and Ro-31-8425 (b) as monitored by the TAMRA/Cy5 emission ratio of the PIC.

ratios decreased with increasing concentrations of the inhibitors. Thus, the inhibitors suppressed the PKCα phosphorylation and the subsequent weakening of the PIC. From these curves, the IC_{50} values of Gö6983 and Ro-31-8425 were determined to be 16 and 24 nM, respectively, which are consistent with the reported values.[33,34]

■ CONCLUSION

We have demonstrated the detection of PKCα activity using a PIC fluorescence probe. This probe was designed to include two fluorescent signals, i.e., an increasing TAMRA signal corresponding to PKCα activity, and a constant Cy5 signal acting as an internal standard. The difference in fluorescence intensities was achieved by adjusting the modification ratio of each fluorophore on the cationic and anionic polymers, respectively. The PIC probe enables quantitative detection of PKCα activity and was successfully applied to the evaluation of PKCα-specific inhibitors. The concept of "internal-signal-embedded probes" will be especially useful for designing probes for intracellular PK activity measurements, where the fluorescence depends on the number of probes transferred into the cell. The fluorescent probe proposed here has difficulty to apply to intracellular activity measurement of PK *in vitro* due to the weakness of the PIC in culture medium and intracellular condition and low cellular uptake. These issues would be overcome by strengthening of the PIC and enhancing the endocytotic uptake by a ligand modification.

■ ASSOCIATED CONTENT

Ⓢ Supporting Information

Experimental details on the preparation and use of cationic and anionic polymers in coupled enzyme assays, measurements of fluorescence intensity, PKCα assays, and inhibitor screening assays.This material is available free of charge via the Internet at http://pubs.acs.org.

■ AUTHOR INFORMATION

Corresponding Author

*Tel/Fax: +81 92 802 2850. E-mail address: ykatatcm@mail.cstm.kyushu-u.ac.jp.

Notes

The authors declare no competing financial interest.

■ ACKNOWLEDGMENTS

This work was financially supported by a Grant-in-aid for Scientific Research form MEXT.

■ ABBREVIATIONS

PK, protein kinase; PIC, polyion complex; PKCα, protein kinase C α

■ REFERENCES

(1) Cohen, P. (2001) The role of protein phosphorylation in human health and disease. *Eur. J. Biochem. 268*, 5001−5010.

(2) Knight, Z. A., Lin, H., and Shokat, K. M. (2010) Targeting the cancer kinome through polypharmacology. *Nat. Rev. Cancer 10*, 130−137.

(3) von Ahsen, O., and Bömer, U. (2005) High-throughput screening for kinase inhibitors. *ChemBioChem 6*, 481−490.

(4) Park, Y. W., Cummings, R. T., Wu, L., Zheng, S., Cameron, P. M., Woods, A., Zaller, D. M., Marcy, A. I., and Hermes, J. D. (1999) Homogeneous proximity tyrosine kinase assays: scintillation proximity assay versus homogeneous time-resolved fluorescence. *Anal. Biochem. 269*, 94−104.

(5) Shiosaki, S., Nobori, T., Mori, T., Toita, R., Nakamura, Y., Kim, C. W., Yamamoto, T., Niidome, T., and Katayama, Y. (2013) A protein kinase assay based on FRET between quantum dots and fluorescently-labeled peptides. *ChemComm 49*, 5592−5594.

(6) Bai, J., Zhao, Y., Wang, Z., Liu, C., Wang, Y., and Li, Z. (2013) Dual-readout fluorescent assay of protein kinase activity by use of TiO_2-coated magnetic microspheres. *Anal. Chem. 85*, 4813−4821.

(7) Honda, K., Yanai, H., Negishi, H., Asagiri, M., Sato, M., Mizutani, T., Shimada, N., Ohba, Y., Takaoka, A., Yoshida, N., and Taniguchi, T. (2005) IRF-7 is the master regulator of type-I interferon-dependent immune responses. *Nature 434*, 772−777.

(8) Sun, H., Low, K. E., Woo, S., Noble, R. L., Graham, R. J., Connaughton, S. S., Gee, M. A., and Lee, L. G. (2005) Real-time protein kinase assay. *Anal. Chem. 77*, 2043−2049.

(9) Toita, R., Mori, T., Naritomi, Y., Kang, J.-H., Shiosaki, S., Niidome, T., and Katayama, Y. (2012) Fluorometric detection of protein kinase Cα activity based on phosphorylation-induced dissociation of a polyion complex. *Anal. Biochem. 424*, 130−136.

(10) Shults, M. D., and Imperiali, B. (2003) Versatile fluorescence probes of protein kinase activity. *J. Am. Chem. Soc. 125*, 14248−14249.

(11) Shults, M. D., Janes, K. A., Lauffenburger, D. A., and Imperiali, B. (2005) A multiplexed homogeneous fluorescence-based assay for protein kinase activity in cell lysates. *Nat. Methods 2*, 277−284.

(12) Shults, M. D., Carrico-Moniz, D., and Imperiali, B. (2006) Optimal Sox-based fluorescent chemosensor design for serine/threonine protein kinases. *Anal. Biochem. 352*, 198−207.

(13) Luković, E., González-Vera, J. A., and Imperiali, B. (2008) Recognition-domain focused chemosensors: versatile and efficient reporters of protein kinase activity. *J. Am. Chem. Soc. 130*, 12821−12827.

(14) Luković, E., Taylor, E. V., and Imperiali, B. (2009) Monitoring protein kinases in cellular media with highly selective chimeric reporters. *Angew. Chem., Int. Ed. 48*, 6828−6831.

(15) Stains, C. I., Tedford, N. C., Walkup, T. C., Luković, E., Goguen, B. N., Griffith, L. G., Lauffenburger, D. A., and Imperiali, B. (2012) Interrogating signaling nodes involved in cellular transformations using kinase activity probes. *Chem. Biol. 19*, 210−217.

(16) Wang, Q., and Lawrence, D. S. (2005) Phosphorylation-driven protein-protein interactions: a protein kinase sensing system. *J. Am. Chem. Soc. 127*, 7684−7685.

(17) Sharma, V., Agnes, R. S., and Lawrence, D. S. (2007) Deep quench: an expanded dynamic range for protein kinase sensors. *J. Am. Chem. Soc. 129*, 2742−2743.

(18) Agnes, R. S., Jernigan, F., Shell, J. R., Sharma, V., and Lawrence, D. S. (2010) Suborganelle sensing of mitochondrial cAMP-dependent protein kinase activity. *J. Am. Chem. Soc. 132*, 6075−6080.

(19) Shell, J. R., and Lawrence, D. S. (2013) Probes of the mitochondrial cAMP-dependent protein kinase. *Biochim. Biophys. Acta 1834*, 1359−1363.

(20) Kim, J.-H., Lee, S., Kim, K., Jeon, H., Park, R.-W., Kim, I.-S., Choi, K., and Kwon, I. C. (2007) Polymeric nanoparticles for protein kinase activity. *Chem. Commun. 13*, 1346−1348.

(21) Kim, J.-H., Lee, S., Park, K., Nam, H. Y., Jang, S. Y., Youn, I., Kim, K., Jeon, H., Park, R.-W., Kim, I.-S., Choi, K., and Kwon, I. C. (2007) Protein-phosphorylation-responsive polymeric nanoparticles for imaging protein kinase activities in single living cells. *Angew. Chem., Int. Ed. 46*, 5779−5782.

(22) Freeman, R., Finder, T., Gill, R., and Willner, I. (2010) Probing protein kinase (CK2) and alkaline phosphatase with CdSe/ZnS quantum dots. *Nano Lett. 10*, 2192−2196.

(23) Ghadiali, J. E., Cohen, B. E., and Stevens, M. M. (2010) Protein kinase-actuated resonance energy transfer in quantum dot-peptide conjugates. *ACS Nano 4*, 4915−4919.

(24) Yuan, L., Lin, W., Zheng, K., and Zhu, S. (2013) FRET-based small-molecule fluorescent probes: rational design and bioimaging applications. *Acc. Chem. Res. 46*, 1462−1473.

(25) Kikuchi, K. (2010) Design, synthesis and biological application of chemical probes for bio-imaging. *Chem. Soc. Rev. 39*, 2048−2053.

(26) Mandil, R., Ashkenazi, E., Blass, M., Kronfeld, I., Kazimirsky, G., Rosenthal, G., Umansky, F., Lorenzo, P. S., Blumberg, P. M., and Brodie, C. (2001) Protein kinase Cα and protein kinase Cδ play opposite roles in the proliferation and apoptosis of glioma cells. *Cancer Res. 61*, 4612−4619.

(27) Mackay, H. J., and Twelves, C. J. (2007) Targeting the protein kinase C family: are we there yet? *Nat. Rev. Cancer 7*, 554−562.

(28) Koga, H., Toita, R., Mori, T., Tomiyama, T., Kang, J.-H., Niidome, T., and Katayama, Y. (2011) Fluorescent nanoparticles consisting of lipopeptides and fluorescein-modified polyanions for monitoring of protein kinase activity. *Bioconjugate Chem. 22*, 1526−1534.

(29) Cook, P. F., Neville, M. E., Jr., Vrana, K. E., Hartl, F. T., and Roskoski, R., Jr. (1982) Adenosine cyclic 3′,5′-monophosphate dependent protein kinase: kinetic mechanism for the bovine skeletal muscle catalytic subunit. *Biochemistry 21*, 5794−5799.

(30) Toita, R., Kang, J.-H., Kim, J.-H., Tomiyama, T., Mori, T., Niidome, T., Jun, B., and Katayama, Y. (2009) Protein kinase Cα-specific peptide substrate graft-type copolymer for cancer cell-specific gene regulation systems. *J. Controlled Release 139*, 133−139.

(31) Popa, I., Gillies, G., Papastavrou, G., and Borkovec, M. (2010) Attractive and repulsive electrostatic forces between positively charged Latex particles in the presence of anionic linear polyelectrolytes. *J. Phys. Chem. B 114*, 3170−3177.

(32) Kang, J.-H., Asami, Y., Murata, M., Kitazaki, H., Sadanaga, N., Tokunaga, E., Shiotani, S., Okada, S., Maehara, Y., Niidome, T., Hashizume, M., Mori, T., and Katayama, Y. (2010) Gold nanoparticle-based colorimetric assay for cancer diagnosis. *Biosens. Bioelectron. 25*, 1869−1874.

(33) Gschwendt, M., Dieterich, S., Rennecke, J., Kittstein, W., Mueller, H.-J., and Johannes, F.-J. (1996) Inhibition of protein kinase C μ by various inhibitors. Differentiation from protein kinase c isoenzymes. *FEBS Lett. 392*, 77−80.

(34) Wilkinson, S. E., Parker, P. J., and Nixon, J. S. (1993) Isoenzyme specificity of bisindolylmaleimides, selective inhibitors of protein kinase C. *Biochem. J. 294*, 335−337.

Mass Spectrometry-Based Metabolic Profiling of Gemcitabine-Sensitive and Gemcitabine-Resistant Pancreatic Cancer Cells

Yoshinori Fujimura, PhD, Naoki Ikenaga, MD, PhD,† Kenoki Ohuchida, MD, PhD,†‡ Daiki Setoyama, PhD,* Miho Irie,§ Daisuke Miura, PhD,* Hiroyuki Wariishi, PhD,*§|| Masaharu Murata, PhD,*‡ Kazuhiro Mizumoto, MD, PhD,†¶ Makoto Hashizume, MD, PhD,*‡ and Masao Tanaka, MD, PhD†*

Objectives: Gemcitabine resistance (GR) is one of the critical issues for therapy for pancreatic cancer, but the mechanism still remains unclear. Our aim was to increase the understanding of GR by metabolic profiling approach.

Methods: To establish GR cells, 2 human pancreatic cancer cell lines, SUIT-2 and CAPAN-1, were exposed to increasing concentration of gemcitabine. Both parental and chemoresistant cells obtained by this treatment were subjected to metabolic profiling based on liquid chromatography-mass spectrometry.

Results: Multivariate statistical analyses, both principal component analysis and orthogonal partial least squares discriminant analysis, distinguished metabolic signature of responsiveness and resistance to gemcitabine in both SUIT-2 and CAPAN-1 cells. Among significantly different ($P < 0.005$) metabolite peaks between parental and GR cells, we identified metabolites related to several metabolic pathways such as amino acid, nucleotide, energy, cofactor, and vitamin pathways. Decreases in glutamine and proline levels as well as increases in aspartate, hydroxyproline, creatine, and creatinine levels were observed in chemoresistant cells from both cell lines.

Conclusions: These results suggest that metabolic profiling can isolate distinct features of pancreatic cancer in the metabolome of gemcitabine-sensitive and GR cells. These findings may contribute to the biomarker discovery and an enhanced understanding of GR in pancreatic cancer.

Key Words: pancreatic cancer, chemoresistance, gemcitabine, metabolic profiling, LC-MS

(*Pancreas* 2014;43: 311–318)

Pancreatic cancer is one of the most lethal cancers, with a 5-year survival rate of only 5%.[1] This poor outcome is caused by difficulty in early detection and limited efficacy of conventional therapeutics including surgical resection, chemotherapy, and radiotherapy. Chemotherapy plays a critical role among pancreatic cancer therapies because 80% to 85% of patients present with unresectable cancer at diagnosis.[1] Gemcitabine and its combination with erlotinib are the current standard treatments of advanced or resected pancreatic cancer; however, the objective response rate and the disease control rate of this treatment approach are 8.0% to 13.5% and 49.2% to 62.1%, respectively.[2,3] Moreover, there are limited options available for second-line treatment after failure of gemcitabine-based regimens.[4] Therefore, we need to develop new therapeutic strategies for gemcitabine-resistant (GR) pancreatic cancer.

Gemcitabine is a specific analogue of the native pyrimidine nucleotide deoxycytidine and a prodrug that requires cellular uptake and intracellular phosphorylation.[5] Gemcitabine transported into cells via human equilibrative nucleoside transporter-1 protein[6] is phosphorylated by deoxycytidine kinase for activation and inhibits DNA synthesis through its incorporation into DNA and inhibition of enzyme ribonucleotide reductase (RR).[7] In addition, deoxyribonucleotide and ribonucleotide pools, both essential for DNA repair, are depleted by the phosphorylated gemcitabine.[8] Conversely, gemcitabine is inactivated intracellularly by cytidine deaminase (CDA).[9] To date, several molecular markers to predict gemcitabine sensitivity, including messenger RNA (mRNA) and microRNA, have been investigated with or without relation to the mechanism of gemcitabine metabolism.[7,10–12] However, the usefulness of such markers in a clinical setting remains unclear because of difficulties in evaluating their protein or mRNA levels, which often degrade during analysis.

Metabolomics is the global or targeted measurement of endogenous metabolite profiles from a biological sample under different conditions. It is a useful approach to understand physiological responses such as cellular metabolic dynamics or cellular signal responses systematically induced by external stimuli (eg, drug treatment).[13] In the cancer research field, metabolomic studies can lead to an enhanced understanding of disease mechanisms and the discovery of new diagnostic biomarkers as well as improved understanding of mechanisms for drug or xenobiotic effects and an increased ability to predict individual variation in drug response phenotypes.[14–20] Moreover, the ability to link the metabolome to phenotype can provide a better understanding of complex biological states, which is important for the development of new therapies.

Recently, studies regarding the metabolic profiling of pancreatic cancer using various types of specimens have been reported. The comparison of metabolic profiles between cancer patients and healthy subjects may allow clinicians to detect an altered pancreatic profile at its early stage and thus enable early diagnosis of pancreatic cancer. In fact, these reports suggested many potential biomarkers of pancreatic cancer in tissue (leucine, isoleucine, valine, lactate, alanine, phosphocholine, glycerophosphocholine, taurine, and betaine[21]; taurine, lactate, creatine, and glutamate[22]), serum

From the *Innovation Center for Medical Redox Navigation; †Departments of Surgery and Oncology, Graduate School of Medical Sciences; ‡Department of Advanced Medical Initiatives, Graduate School of Medical Sciences; §Faculty of Agriculture; ||Bio-Architecture Center, Kyushu University, Fukuoka, Japan; and ¶Kyushu University Hospital Cancer Center, Fukuoka, Japan.

Received for publication December 14, 2012; accepted August 1, 2013.

Reprints: Yoshinori Fujimura, PhD, Innovation Center for Medical Redox Navigation, Kyushu University, 3-1-1 Maidashi, Higashi-ku, Fukuoka 812-8582 Japan (e-mail: fujimu@redoxnavi.med.kyuhsu-u.ac.jp).

Yoshinori Fujimura and Naoki Ikenaga equally contributed to this work.

Naoki Ikenaga is a research fellow of the Japan Society for the Promotion of Science.

This work was supported by the Project for Developing Innovation Systems Creation of Innovation Centers for Advanced Interdisciplinary Research Areas Program and a Grant-in-Aid from the Ministry of Education, Culture, Sports, Science and Technology of Japan.

The authors declare no conflict of interest.

Supplemental digital contents are available for this article. Direct URL citations appear in the printed text and are provided in the HTML and PDF versions of this article on the journal's Web site (www.pancreasjournal.com).

(3-hydroxybutyrate, 3-hydroxyisovalerate, lactate, trimethylamine-*N*-oxide, isoleucine, triglyceride, leucine, and creatine[23]; glutamate, acetone, 3-hydroxybutyrate, glucose, phenylalanine, formate, mannose, ethanol, asparagine, creatine, proline, and glycerol[24]), plasma (*N*-methylalanine, lysine, glutamine, phenylalanine, arachidonic acid, lysoPC [18:2], phosphatidylcholine [34:2], phosphatidylethanolamine [26:0], tauroursodeoxycholic acid, taurocholic acid, deoxycholylglycine, and cholylglycine),[25] urine (acetoacetate, citrate, creatinine, glucose, glycine, hippurate, 3-hydoxyisovalerate, leucine, 2-phenylacetamide, and trigonelline[26]), and saliva (leucine, isoleucine, tryptophan, valine, glutamate, phenylalanine, glutamine, and aspartate).[27] Therefore, metabolomics approach targeting water-soluble (polar) metabolites observed in many of the above-mentioned potential biomarkers may be beneficial for the biomarker discovery and an enhanced metabolic understanding of pancreatic cancer. On the other hand, chemoresistance such as GR is one of the critical issues for therapy for pancreatic cancer, but metabolomics-based study in this context has not yet been reported. To obtain a potential metabolomic understanding of chemoresistance in pancreatic cancer, we performed hydrophilic metabolic profiling of both gemcitabine-sensitive and GR cells.

MATERIALS AND METHODS

Cell Lines and Establishment of GR Cells

Two human pancreatic cancer cell lines, SUIT-2 and CAPAN-1 (gift from Dr H. Iguchi, National Shikoku Cancer Center, Matsuyama, Japan), were used in this study. Gemcitabine-resistant cells were generated by exposing both cell lines to gradually increasing concentrations of gemcitabine dissolved in phosphate-buffered saline (Wako Pure Chemical Industries, Osaka, Japan). The initial concentration of gemcitabine was 1 nM, which did not seem to affect the proliferation of either SUIT-2 or CAPAN-1 cells. When the cells had adapted to the drug, the concentration of gemcitabine was gradually increased by 10 to 100 nM per week to a final concentration of 200 nM (SUIT-2) and 1 μM (CAPAN-1). Cells were maintained in Dulbecco's modified Eagle medium (Sigma-Aldrich, St Louis, Mo) supplemented with 10% fetal bovine serum, streptomycin (100 μg/mL), and penicillin (100 μg/mL) at 37°C in a humidified atmosphere containing 10% CO_2. After establishment of GR cells (GR SUIT-2 [SUIT-2-GR] and GR CAPAN-1 [CAPAN-1-GR]), the cells were cultured in gemcitabine-free normal medium for more than 10 days. We used the cultured cells for further experiments.

Propidium Iodide Assay

Cells were seeded in 24 well culture plates (Becton-Dickinson Labware, Bedford, Mass) at 2×10^4 per well, using cell numbers previously counted using a particle distribution analyzer (CDA500; Sysmex, Kobe, Japan). Several different concentrations of gemcitabine were added to the cells 24 hours after seeding, and the cells were incubated for 72 hours. Propidium iodide (PI) (30 μM) and digitonin (600 μM) were added to each well to label all nuclei with PI. Cell proliferation was evaluated by measuring the fluorescence intensity of PI with an Infinite F200 (TECAN, Männedorf, Switzerland). The results were converted to percentage survival rates by comparing treated cells with untreated cells, and the 50% inhibitory concentration of gemcitabine for SUIT-2 and CAPAN-1 cells was calculated.

Extraction of Metabolites in Cancer Cell Lines

Metabolites were extracted using a modified extraction protocol, as described previously.[28] Cells were cultured in 90-mm dishes to confluent monolayer (>1×10^7 cells) and washed twice with cold phosphate-buffered saline. After addition of 1 mL of cold methanol containing 100 μM of 2,2-dimethyl succinic acid and 2-hydroxyundecanoic acid (for evaluating the extraction efficiency), cells were scraped on ice and sonicated for 5 minutes on ice. After centrifugation at 15,000 × *g* for 20 minutes, the supernatant was collected, and an equal volume of a 2:1 $H_2O/CHCl_3$ solution was added and mixed vigorously for 30 seconds. Each sample was then centrifuged at 15,000 × *g* for 20 minutes at 4°C. After centrifugation, the aqueous layers were collected. A SpeedVac Concentrator (Savant Instruments Inc, Holbrook, NY) was used for solvent removal and sample concentration. The resultant samples were stored at −80°C until assay.

Liquid Chromatography-Mass Spectrometry Analysis

Samples were diluted in 80 μL of 2.2 mM ammonium formate and 75% acetonitrile solution, including 600 μM sulfanilamide as an internal standard, and measured by high-performance liquid chromatography (LC) with time-of-flight mass spectrometry (MS) (LCMS-IT-TOF; Shimadzu Corporation, Kyoto, Japan). The instrument was fitted with a hydrophilic interaction LC column (ZIC-*p*HILIC column 150 × 2.1 mm, 5μm; Merck Biosciences, San Diego, Calif) maintained at 40°C. Mobile phase conditions were as follows: linear gradient analysis with mobile phase A, 6.5 mM of ammonium formate, and mobile phase B, 100% acetonitrile. After a 1-minute isocratic run at 90% of the eluting solvent B, the ratio of eluting solvent B was linearly decreased to 60% from 1 to 4 minutes and to 10% from 4 to 6 minutes. The composition of 10% of the eluting solvent B was maintained for 10 minutes. The ratio of eluting solvent B was linearly increased to 90% from 16 to 18 minutes, and the column equilibration was carried out with 90% of the eluting solvent B for 7 minutes. A 3-μL aliquot of the sample solution filtered through a 0.22-μm syringe (Milliex-GV; Millipore, Billerica, Mass) was injected into the column with a flow rate of 0.15 mL/min. For MS condition, the instrument was operated using an electrospray ionization source in both positive and negative ionization modes with survey scans acquired from *m/z* 50 to 800. The ionization parameters were as follows: capillary voltage, 4.5 and −3.5 kV; nebulizer gas flow, 1.5 L/min; curved desolvation line and heat block temperature, 250°C.

Multivariate Statistical Analysis

Mass spectra data obtained by LC-MS were processed using Profiling Solution software (Shimadzu Corporation, Kyoto, Japan) to extract and align peaks. All *m/z* peaks (variables) in either positive or negative ionization mode were separately normalized to the total ion counts (TICs) of each sample. After the integration of both TIC-normalized variables, these data were filtered by the 2 criteria; at least 1 group of parental (P) or GR cells (n = 10) satisfied both missing values less than 25% and intragroup relative standard deviation values less than 75%. All variables were mean centered and scaled to Pareto variance. Two types of cells (P and GR) were evaluated by multivariate statistical analysis, which was generally used to clarify similarities and differences among samples on the basis of multivariate data (eg, MS data sets). Here, we carried out an unsupervised multivariate analysis, principal component analysis (PCA),[29] using SIMCA-P+ version 13 (Umetrics, Umea, Sweden). Principal component analysis models are depicted as score plots and consist of 2 synthetic variables: principal component (PC) 1 (the greatest variance of data) and PC2 (the second greatest variance of data, orthogonal with PC1). These display intrinsic groups of samples based on spectral variations. This analysis can explain the original features of samples based on the ratio of the sum of percentages of PC1 and PC2. Although the PCA model can provide an overview of all observations or samples, the details of differences in each

cluster remain unclear. Therefore, the supervised method, orthogonal partial least squares discriminant analysis (OPLS-DA), was then used to evaluate for potential differences between P and GR cells. The goodness-of-fit parameter R^2 and the predictive ability parameter Q^2 were 0.999 and 0.993, respectively (SUIT-2), or 0.988 and 0.977, respectively (CAPAN-1). The quality of OPLS-DA models was evaluated by both R^2 and Q^2 values. The value higher than 0.5 indicates good quality of OPLS-DA models. Therefore, the present data indicated that the OPLS-DA models were reliable. Metabolite peaks were assigned by MS/MS analysis or by searching their accurate masses using online metabolite databases (KEGG, METLIN, HMDB, or MassBank).

Volcano Plot Analysis

Data sets normalized and filtered by TIC were subjected to a 2-sided Welch *t* test, assuming equal means and unequal variance. Significance level was set at each side to 0.005%. The data sets were all mean centered and scaled to Pareto. Variables, transformed into the binary; −log10 (*P* values); and the mean difference of the scaled values (mean GR − mean P) were represented as volcano plots.

RESULTS

Establishment of GR Pancreatic Cancer Cells

Gemcitabine-resistant SUIT-2 and CAPAN-1-GR cells were generated from P cell lines (SUIT-2-P and CAPAN-1-P). The viability of SUIT-2-P and CAPAN-1-P significantly decreased to less than 10% after treatment with 10 nM and 300 nM of gemcitabine, respectively, whereas the viability of SUIT-2-GR and CAPAN-1-GR remained unchanged after treatment with 10 nM and 300 nM of gemcitabine, respectively (Fig. 1). The gemcitabine 50% inhibitory concentration values for SUIT-2-GR and CAPAN-1-GR were significantly higher than those of the P cells ($P < 0.001$; 8,576.1 ± 156.4 nM in SUIT-2-GR vs 2.8 ± 0.2 nM in SUIT-2-P and 23,520.7 ± 680.7 nM in CAPAN-1-GR vs 62.6 ± 5.3 nM in CAPAN-1-P). We used these P cells and established GR cells in the subsequent experiments.

Unsupervised Evaluation of Metabolite Signatures of Gemcitabine-Sensitive and GR Pancreatic Cancer Cells by PCA

To provide comparative interpretations and to visualize metabolic similarities or differences between P and GR cells in relation to their sensitivity to gemcitabine, we analyzed the LC-MS spectra data sets (SUIT-2: 703 peaks; CAPAN-1: 584 peaks) using multivariate analysis. An unsupervised multivariate analysis, PCA, provides an overview of all observations or samples in a data set.[29] In addition, groupings, trends, and outliers can also be found. As shown in Figure 2A, the results of a PCA score plot in PC1/PC2 (SUIT-2: 29.8%/8.2%; CAPAN-1: 27.0%/13.1%) clearly demonstrated that independent clusters were formed between P and GR groups in both SUIT-2 and CAPAN-1 cells. Furthermore, a supervised multivariate analysis, OPLS-DA, also showed a clear separation of groups in both cell lines (Fig. 2B). Information on metabolite peaks that contributed to the construction of the OPLS-DA model is available in the supplemental section (see Table, Supplemental Digital Content 1, http://links.lww.com/MPA/A270). These data indicate that the metabolic profiles of pancreatic cancer cells are clearly different on the basis of gemcitabine sensitivity.

Analysis of Metabolite Peaks Correlated With Gemcitabine Sensitivity

To investigate metabolic differences between P and GR groups in SUIT-2 and CAPAN-1 cells, we created volcano plots (Fig. 3), which can highlight statistically different variables between the 2 groups. The plot displayed the mean difference and *P* values in the data sets of P and GR cells. In SUIT-2 cells, 34.4% (242 peaks) of all peaks (703 peaks) were significantly different ($P < 0.005$) between P and GR cells, with 133 being higher in P cells and 109 being higher in GR cells. In CAPAN-1 cells, 33.0% (193 peaks) of all peaks (584 peaks) were significantly different ($P < 0.005$) between both cells; 58 were higher in the P group and 135 were higher in the GR group. As shown in Figure 4, although most peaks were cell line–specific peaks, 8 peaks, which were reduced in GR cells compared with P cells, were common to both the SUIT-2 and CAPAN-1 cell lines. In the case of peaks enhanced in GR cells, 15 were common to both SUIT-2 and CAPAN-1 cell lines. Among these significantly altered peaks ($P < 0.005$), identified peaks were shown as table (Tables 1, 2) and box-and-whisker plot (see Figure, Supplemental Digital Content 2, http://links.lww.com/MPA/A271 and Supplemental Digital Content 3, http://links.lww.com/MPA/A272). Metabolites related to several metabolic pathways such as amino acid, nucleotide, energy, cofactor, and vitamin pathways were observed. In the case of metabolites reduced in GR cells (Table 1, Supplemental Digital Content 2, http://links.lww.com/MPA/A271), the number of metabolites (SUIT-2 or CAPAN-1) was 11 or 13, respectively. The SUIT-2–specific metabolites were 5-methylcytidine, citrulline, phenylalanine, cytidine, cysteine-glutathione disulfide, methionine, tryptophan, histidine, and valine. The CAPAN-1–specific metabolites were 1-aminocyclopropane-1-carboxylate, glutathione (GSH), *S*-methylglutathione, glutamate, uridine, cytidine 5′-monophosphate (CMP), *myo*-inositol, adenosine 5′-monophosphate (AMP), quinolinate, malate, and deoxyguanosine

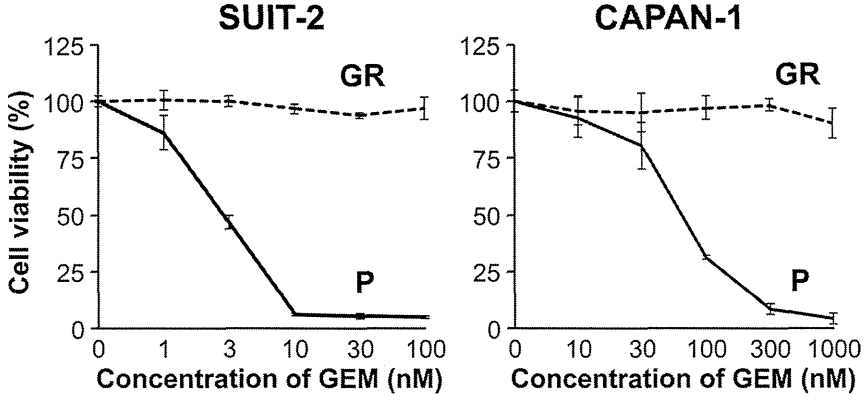

FIGURE 1. Viability of P and GR cells exposed to gemcitabine (GEM). GR cells, SUIT-2-GR and CAPAN-1-GR, were significantly more resistant to gemcitabine than the P cells, SUIT-2-P and CAPAN-1-P.

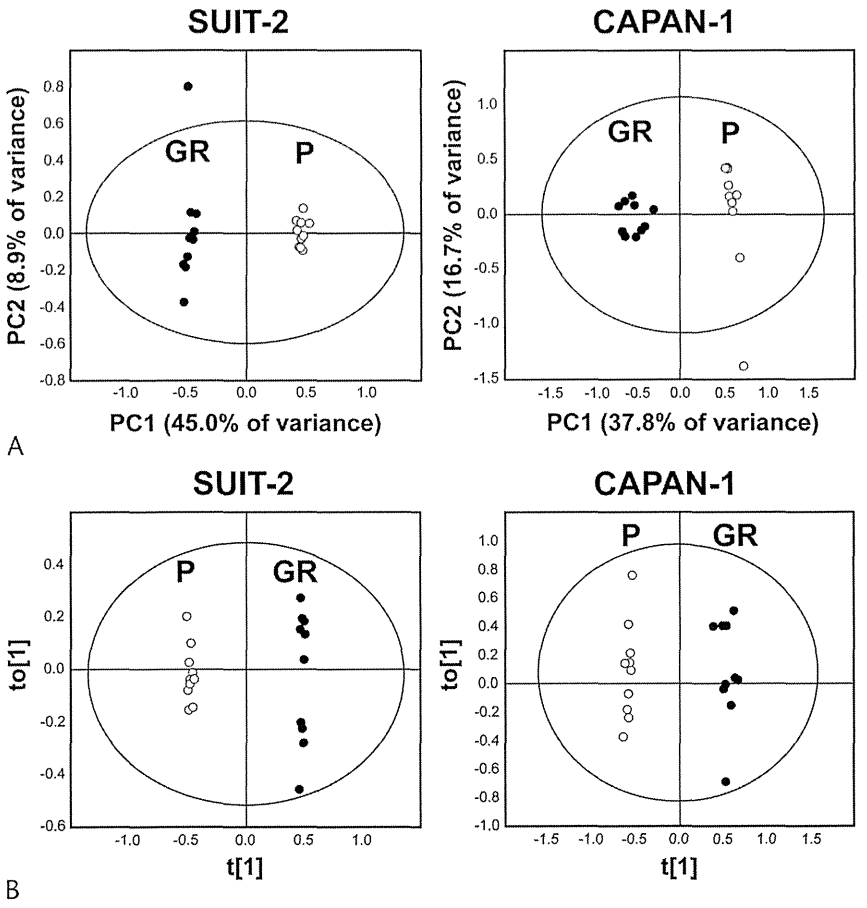

FIGURE 2. PCA and OPLS-DA score plots based on metabolite profiles obtained from LC-MS analysis of pancreatic cells. The unsupervised PCA (A) and the supervised OPLS-DA (B) score plots were generated using each LC-MS data set. Open circle and closed circle indicate P and GR cells, respectively. The score plot shows separate clustering of MS profiles of the 2 cells.

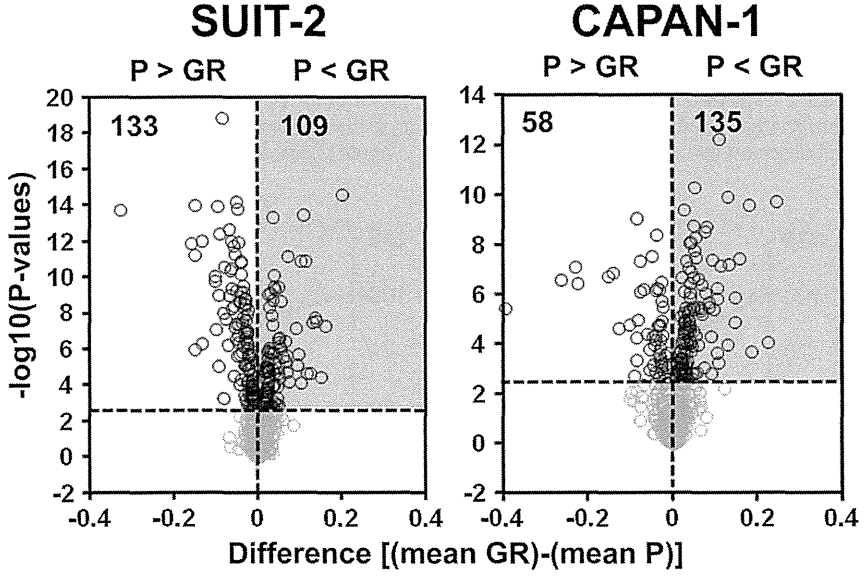

FIGURE 3. Volcano plots displaying the mean difference and *P* values in data sets of P and GR cells. Horizontal broken line indicates a significant difference ($P < 0.005$) between the P and GR groups. In both cell lines, more than 30% of all peaks were statistically significantly different when comparing the P and GR groups.

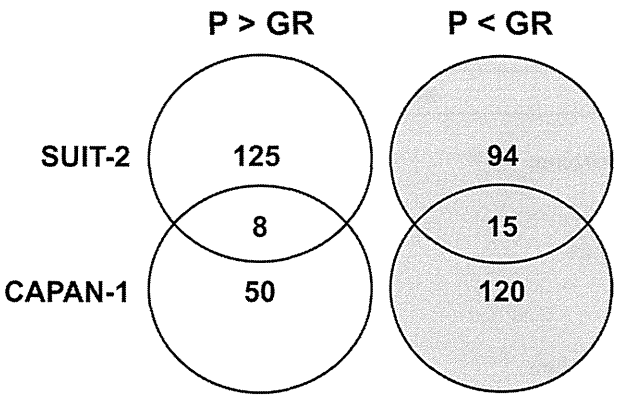

FIGURE 4. Venn diagram illustrating proportion of unique and overlapping ion peak features in SUIT-2 and CAPAN-1.

5′-diphosphate. Two metabolites, glutamine and proline, were common to both SUIT-2 and CAPAN-1 cells. In the case of peaks enhanced in GR cells (Table 2, Supplemental Digital Content 3, http://links.lww.com/MPA/A272), the number of metabolites (SUIT-2 or CAPAN-1) was 12 or 17, respectively. The SUIT-2–specific metabolites were *O*-acetylserine, glutamate, *S*-methylglutathione, betaine, CMP, GSH, adenosine 5′-monophosphate, and sebacate. The CAPAN-1–specific metabolites were cytidine, 5-methylcytidine, hypotaurine, *N*-acetyl-aspartyl-glutamate (NAAG), dihydrobiopterin, 2-aminobutyrate, L-homoserine, 5-methyldeoxycytidine, stachydrine, citrate, inosine 5′-monophosphate, β-alanine, and glucose 6-phosphate. Four metabolites (creatine, hydroxyproline, aspartate, and creatinine) were common to both cell lines. These metabolites contribute to the difference in metabolic states associated with gemcitabine sensitivity in SUIT-2 and CAPAN-1 cells.

DISCUSSION

We found several common metabolites associated with gemcitabine sensitivity in 2 human pancreatic ductal adenocarcinoma lines, SUIT-2 and CAPAN-1. In chemoresistant cells, proline and glutamine were decreased, whereas aspartate, hydoxyproline, creatine, and creatinine were increased (Tables 1, 2). These metabolites have the potential to act as molecular markers for discriminating between gemcitabine-sensitive and GR pancreatic cancer cells. Although several molecular markers such as transcripts and proteins have been reported,[7,10–12] this is the first report identifying metabolites with low molecular weight possibly contributing to the prediction of gemcitabine sensitivity. Quantitative analysis of metabolic products is expected to be a useful tool in a clinical setting. Further investigations are required to establish whether the alterations of metabolites identified here are observed in clinical pancreatic cancer tissues and whether these correlate with information regarding sensitivity to gemcitabine.

Cancer cells possess a unique metabolic phenotype, which is characterized by high glucose uptake, increased glycolytic activity, decreased mitochondrial activity, low bioenergetics, high glutaminase

TABLE 1. Significantly Altered Metabolites (P > GR)

Metabolite	Metabolic Pathway	Relative Ratio (GR/P)	*P* (P vs GR)
SUIT-2			
5-Methylcytidine	Pyrimidine metabolism	0.23	1.37×10^{-19}
Glutamine	Glutamate metabolism	0.56	5.94×10^{-12}
Citrulline	Urea cycle, arginine and proline	0.66	9.84×10^{-10}
Proline	Urea cycle, arginine and proline	0.77	2.49×10^{-7}
Phenylalanine	Phenylalanine and tyrosine metabolism	0.80	5.54×10^{-7}
Cytidine	Pyrimidine metabolism	<0.01	6.71×10^{-6}
Cytidine-glutathione disulfide	Glutathione metabolism	0.75	8.87×10^{-6}
Methionine	Cysteine, methionine, SAM, and taurine	0.70	6.31×10^{-5}
Tryptophan	Tryptophan metabolism	0.82	9.04×10^{-5}
Histidine	Histidine metabolism	0.89	5.09×10^{-4}
Valine	Valine, leucine, and isoleucine	0.76	4.25×10^{-3}
CAPAN-1			
1-Aminocyclopropane-1-carboxylate	Cysteine, methionine, SAM, and taurine	0.45	2.82×10^{-8}
GSH	Glutathione metabolism	0.32	1.89×10^{-7}
Glutamine	Glutamate metabolism	0.05	2.57×10^{-7}
S-Methylglutathione	Glutathione metabolism	0.21	3.25×10^{-7}
Glutamate	Glutamate metabolism	0.67	3.68×10^{-7}
Uridine	Pyrimidine metabolism	<0.01	1.59×10^{-5}
CMP	Pyrimidine metabolism	0.07	5.49×10^{-5}
myo-Inositol	Inositol metabolism	<0.01	6.80×10^{-5}
AMP	Purine metabolism	<0.01	1.40×10^{-4}
Quinolinate	Nicotinate and nicotinamide metabolism	0.15	6.18×10^{-4}
Proline	Urea cycle, arginine and proline	0.08	8.36×10^{-4}
Malate	TCA cycle, nicotinate and nicotinamide	0.45	1.01×10^{-3}
dGDP	Purine metabolism	0.65	3.95×10^{-3}

Values are presented as the relative ratio of TIC-normalized peak intensity for the GR cells against that of the P cells (n = 10). *P* values were calculated using Welch *t* test (P vs GR) in SUIT-2 and CAPAN-1 cells. The bold font indicates metabolites common to both cell lines.

SAM indicates *S*-adenosylmethionine.

TABLE 2. Significantly Altered Metabolites (P < GR)

Metabolite	Metabolic Pathway	Relative Ratio (GR/P)	*P* (P vs GR)
SUIT-2			
O-Acetylserine	Glycine, serine, and threonine metabolism	1.80	6.61×10^{-12}
Creatine	Creatine metabolism	3.25	2.76×10^{-8}
Hydroxyproline	Urea cycle, arginine and proline	3.54	4.75×10^{-6}
Aspartate	Alanine and aspartate metabolism	3.18	6.51×10^{-6}
Creatinine	Creatine metabolism	1.42	1.74×10^{-5}
Glutamate	Glutamate metabolism	1.27	2.06×10^{-5}
S-Methylglutathione	Glutathione metabolism	2.19	6.21×10^{-5}
Betaine	Glycine, serine, and threonine metabolism	2.61	1.17×10^{-3}
CMP	Pyrimidine metabolism	1.15	1.47×10^{-3}
GSH	Glutathione metabolism	1.24	2.48×10^{-3}
AMP	Purine metabolism	2.38	2.99×10^{-3}
Sebacate	Fatty acid, dicarboxylate metabolism	1.72	4.29×10^{-3}
CAPAN-1			
Cytidine	Pyrimidine metabolism	65.14	1.18×10^{-10}
5-Methylcytidine	Pyrimidine metabolism	2.17	1.81×10^{-10}
Hypotaurine	Cysteine, methionine, SAM, and taurine	26.47	4.24×10^{-10}
NAAG	Glutamate metabolism	1.79	1.82×10^{-9}
Dihydrobiopterin	Folate metabolism	5.88	1.75×10^{-8}
2-Aminobutyrate	Butanoate metabolism	2.54	2.07×10^{-7}
Aspartate	Alanine and aspartate metabolism	2.25	5.85×10^{-7}
L-Homoserine	Glycine, serine, and threonine metabolism	1.42	3.23×10^{-6}
5-Methyl-2′-deoxycytidine	Pyrimidine metabolism	>100	3.81×10^{-6}
Stachydrine	Urea cycle, arginine and proline	4.64	5.46×10^{-6}
Citrate	TCA cycle	3.28	8.32×10^{-5}
Inosine 5'-monophosphate	Purine metabolism	4.15	6.15×10^{-4}
β-Alanine	Alanine and aspartate metabolism	1.28	8.14×10^{-4}
Glucose 6-phosphate	Glycolysis, pyruvate metabolism	>100	1.43×10^{-3}
Hydroxyproline	Urea cycle, arginine and proline	3.78	2.22×10^{-3}
Creatine	Creatine metabolism	1.43	3.31×10^{-3}
Creatinine	Creatine metabolism	6.25	3.44×10^{-3}

Values are presented as the relative ratio of TIC-normalized peak intensity for the GR cells against that of the P cells (n = 10). *P* values were calculated using Welch *t* test (P vs GR) in SUIT-2 and CAPAN-1 cells. The bold font indicates metabolites common to both cell lines.

activity, and increased phospholipid turnover.[19,30,31] Glutamine is a preferred amino acid for energy generation by cancer cells,[32] in which high glutaminase activity and low glutamine synthase activity have been observed.[33] In tumor tissues, conversion of glutamine to glutamate is enhanced and glutamate is the most abundant amino acid. The transcription factor c-*Myc*, which links altered cellular metabolism to tumorigenesis, can stimulate glycolysis and glutamine metabolism through the upregulation of glycolysis-related pyruvate kinase and glutaminase, respectively.[34] Decreased glutamine and increased glutamate levels observed in SUIT-2-GR cells may be due to an alteration of glycolytic and glutaminase activities. In CAPAN-1-GR cells, decreased glutamine and increased β-alanine levels were shown. This finding also indicates alteration of glycolytic activity because lactate and β-alanine accumulate as a by-product of increased glycolytic activity.[19,30,31]

Aspartate, glutamate, and malate are interconverted through malate-aspartate shuttle and tricarboxylic acid (TCA) cycle. Aspartate is involved in glutamate and DNA metabolisms and urea cycle, and NAAG generated by aspartate and glutamate is highly expressed in pancreatic tissues.[35] Glutamate can also be converted directly into GSH and contributes to the maintenance of balanced cellular redox status.[34] Increased levels of aspartate in GR cells observed here may reflect the development of tolerance to redox stress provided by gemcitabine. On the other hand, both p53 and c-*Myc*, which are oncogenes in pancreatic cancer,[36,37] are essential transcription factors regulating enzymes of central metabolite pathways (glycolysis and TCA cycle).[34,38] These are involved in the mutual regulation of microRNA-34a[39–41] that may be responsible for GR in pancreatic cancer[42] and inversely associate with gemcitabine sensitivity in both SUIT-2 and CAPAN-1 cells, as we previously reported.[12] Nuclear factor–κB, a contributor to the GR in pancreatic cancer cells,[43] also regulates microRNA-34a[43] and the central metabolic pathway coordinately with p53.[44] Elucidating the potential interrelationship among a series of metabolites, microRNA, and transcription factors may lead to further understanding of the complex mechanisms of GR in pancreatic cancer.

Proline and its posttranslational product, hydroxyproline, are abundant in tumor tissues[45] and involved in biosynthesis of fatty acids and nucleic acids.[46,47] The metabolism of proline as a stress substrate modulates carcinogenic pathways and is responsible for the increased production of intracellular reactive oxygen species (ROS) mediated though p53-induced proline oxidase.[46,47] Previously, levels of intracellular ROS in gemcitabine-sensitive KLM1 pancreatic cancer cells were found to be increased by gemcitabine exposure, and the basal ROS level of GR cells was

higher than that of gemcitabine-sensitive cells.[48] Furthermore, H_2O_2-induced cytotoxic effects were clearly suppressed in GR cells as compared with gemcitabine-sensitive cells, suggesting that the former had acquired potent resistance to oxidative stress.[48] Reduced levels of proline and increased levels of hydroxyproline in GR cells may be, in part, due to an alteration of intracellular redox status as well as biosynthesis of nucleic acids and fatty acids based on proline metabolism.

Creatine, creatinine, aspartate, and citrulline are representative metabolites related to urea cycle and are involved in the production of nitric oxide (NO). Creatine is synthesized from arginine, glycine, and methionine and is also converted to creatinine. This pathway is related to glutamate and proline metabolisms, regulating bioenergetics and redox status.[49] Hydrobiopterin is one of the major components of folate metabolism and an oxidative stress-induced product of tetrahydrobiopterin. The balance of such biopterins contributes to the NO synthase–mediated production of NO and superoxide.[50] Although there are no reports regarding the abovementioned metabolites in pancreatic cancer, increased levels of creatine, creatinine, and aspatate in GR cells may imply the potential relationship between our described metabolite pathways, proline, glutamate, and folate metabolisms, and GR in pancreatic cancer.

In this study, CAPAN-1 had a higher resistance to gemcitabine compared with SUIT-2 (Fig. 1). Our previous works also revealed that mRNA expression of GR-related RR in CAPAN-1 was higher than in SUIT-2, and the level was reduced in CAPAN-1-GR cells.[51] Ribonucleotide reductase is an enzyme catalyzing conversion of ribonucleotide to deoxyribonucleotide,[7] and decreased deoxyguanosine 5′-diphosphate (dGDP) level in CAPAN-1-GR cells (Table 1) may be due to decreased expression of RR. This enzyme is also regulated by p53 and NO,[52] and further investigation of the relationship between RR-related metabolism and the abovementioned metabolites is required for a better understanding of GR. Another GR-related enzyme, CDA, can catalyze conversion of deoxycytidine to deoxyuridine and cytidine to uridine.[7,53] In this study, decreased uridine and CMP as well as increased cytidine levels in CAPAN-1-GR cells were observed, and this may be attributed to the reduced activity of CDA and enhanced conversion of CMP to cytidine. Previously, we reported that mRNA expression of CDA in SUIT-2 was increased in GR.[51] Although a significant increase in uridine in SUIT-2-GR cells was not observed, decreased cytidine and CMP levels may be due to the enhanced activity of CDA and conversion of CMP to cytidine.

In conclusion, we showed the possibility to isolate distinct features of pancreatic cancer in the metabolome of gemcitabine-sensitive and GR cells by metabolic profiling. The available data are still not sufficient to confirm the suitability of different cells and tissues in the diagnosis of chemoresistance, and more extensive analyses of pancreatic cancer samples are needed. In the future, advanced understanding of metabolic alterations associated with gemcitabine sensitivity and discovery of a perturbation method for metabolic profiles may lead to a new option for preventing the acquisition of chemoresistance and improving acquired resistance in pancreatic cancer.

ACKNOWLEDGMENTS

The authors thank Shimadzu Corporation for its full cooperation and Emiko Manabe (Kyusyu University) for skillful technical assistance.

REFERENCES

1. Vincent A, Herman J, Schulick R, et al. Pancreatic cancer. *Lancet.* 2011;378:607–620.
2. Moore MJ, Goldstein D, Hamm J, et al. Erlotinib plus gemcitabine compared with gemcitabine alone in patients with advanced pancreatic cancer: a phase III trial of the National Cancer Institute of Canada Clinical Trials Group. *J Clin Oncol.* 2007;25:1960–1966.
3. Van Cutsem E, Vervenne WL, Bennouna J, et al. Phase III trial of bevacizumab in combination with gemcitabine and erlotinib in patients with metastatic pancreatic cancer. *J Clin Oncol.* 2009;27:2231–2237.
4. Makrilia N, Syrigos KN, Saif MW. Treatment for refractory pancreatic cancer. Highlights from the "2011 ASCO Gastrointestinal Cancers Symposium". San Francisco, CA, USA. January 20–22, 2011. *JOP.* 2011;12:110–113.
5. Mini E, Nobili S, Caciagli B, et al. Cellular pharmacology of gemcitabine. *Ann Oncol.* 2006;17(suppl 5):v7–v12.
6. Garcia-Manteiga J, Molina-Arcas M, Casado FJ, et al. Nucleoside transporter profiles in human pancreatic cancer cells: role of hCNT1 in 2′,2′-difluorodeoxycytidine- induced cytotoxicity. *Clin Cancer Res.* 2003;9:5000–5008.
7. Ueno H, Kiyosawa K, Kaniwa N. Pharmacogenomics of gemcitabine: can genetic studies lead to tailor-made therapy? *Br J Cancer.* 2007;97:145–151.
8. Heinemann V, Xu YZ, Chubb S, et al. Cellular elimination of 2′,2′-difluorodeoxycytidine 5′-triphosphate: a mechanism of self-potentiation. *Cancer Res.* 1992;52:533–539.
9. Eda H, Ura M, FO K, et al. The antiproliferative activity of DMDC is modulated by inhibition of cytidine deaminase. *Cancer Res.* 1998;58:1165–1169.
10. Mahon PC, Baril P, Bhakta V, et al. S100a4 contributes to the suppression of BNIP3 expression, chemoresistance, and inhibition of apoptosis in pancreatic cancer. *Cancer Res.* 2007;67:6786–6795.
11. Ali S, Ahmad A, Banerjee S, et al. Gemcitabine sensitivity can be induced in pancreatic cancer cells through modulation of miR-200 and miR-21 expression by curcumin or its analogue cdf. *Cancer Res.* 2010;70:3606–3617.
12. Ohuchida K, Mizumoto K, Kayashima T, et al. Microrna expression as a predictive marker for gemcitabine response after surgical resection of pancreatic cancer. *Ann Surg Oncol.* 2011;18:2381–2387.
13. Nicholson JK, Lindon JC, Holmes E. 'Metabonomics': understanding the metabolic responses of living systems to pathophysiological stimuli via multivariate statistical analysis of biological NMR spectroscopic data. *Xenobiotica.* 1999;29:1181–1189.
14. Griffin JL, Shockcor JP. Metabolic profiles of cancer cells. *Nat Rev Cancer.* 2004;4:551–561.
15. Soga T, Baran R, Suematsu M, et al. Differential metabolomics reveals ophthalmic acid as an oxidative stress biomarker indicating hepatic glutathione consumption. *J Biol Chem.* 2006;281:16768–16776.
16. Holmes E, Wilson ID, Nicholson JK. Metabolic phenotyping in health and disease. *Cell.* 2008;134:714–717.
17. Denkert C, Budczies J, Kind T, et al. Mass spectrometry–based metabolic profiling reveals different metabolite patterns in invasive ovarian carcinomas and ovarian borderline tumors. *Cancer Res.* 2006;66:10795–10804.
18. Sreekumar A, Poisson LM, Rajendiran TM, et al. Metabolomic profiles delineate potential role for sarcosine in prostate cancer progression. *Nature.* 2009;457:910–914.
19. Merz AL, Serkova NJ. Use of nuclear magnetic resonance-based metabolomics in detecting drug resistance in cancer. *Biomark Med.* 2009;3:289–306.
20. Klawitter J, Kominsky DJ, Brown JL, et al. Metabolic characteristics of imatinib resistance in chronic myeloid leukaemia cells. *Br J Pharmacol.* 2009;158:588–600.
21. Fang F, He X, Deng H, et al. Discrimination of metabolic profiles of pancreatic cancer from chronic pancreatitis by high-resolution magic angle spinning 1H nuclear magnetic resonance and principal components analysis. *Cancer Sci.* 2007;98:1678–1682.
22. Kaplan O, Kushnir T, Askenazy N, et al. Role of nuclear magnetic resonance spectroscopy (MRS) in cancer diagnosis and treatment: 31P, 23Na, and 1h MRS studies of three models of pancreatic cancer. *Cancer Res.* 1997;57:1452–1459.

23. OuYang D, Xu J, Huang H, et al. Metabolomic profiling of serum from human pancreatic cancer patients using 1H NMR spectroscopy and principal component analysis. *Appl Biochem Biotechnol.* 2011;165:148–154.
24. Bathe OF, Shaykhutdinov R, Kopciuk K, et al. Feasibility of identifying pancreatic cancer based on serum metabolomics. *Cancer Epidemiol Biomarkers Prev.* 2011;20:140–147.
25. Urayama S, Zou W, Brooks K, et al. Comprehensive mass spectrometry based metabolic profiling of blood plasma reveals potent discriminatory classifiers of pancreatic cancer. *Rapid Commun Mass Spectrom.* 2010;24:613–620.
26. Napoli C, Sperandio N, Lawlor RT, et al. Urine metabolic signature of pancreatic ductal adenocarcinoma by (1)h nuclear magnetic resonance: identification, mapping, and evolution. *J Proteome Res.* 2012;11:1274–1283.
27. Sugimoto M, Wong DT, Hirayama A, et al. Capillary electrophoresis mass spectrometry-based saliva metabolomics identified oral, breast and pancreatic cancer-specific profiles. *Metabolomics.* 2010;6:78–95.
28. Miura D, Fujimura Y, Yamato M, et al. Ultrahighly sensitive in situ metabolomic imaging for visualizing spatiotemporal metabolic behaviors. *Anal Chem.* 2010;82:9789–9796.
29. Trygg J, Holmes E, Lundstedt T. Chemometrics in metabonomics. *J Proteome Res.* 2007;6:469–479.
30. Israel M, Schwartz L. The metabolic advantage of tumor cells. *Mol Cancer.* 2011;10:70.
31. Fantin VR, St-Pierre J, Leder P. Attenuation of LDH-A expression uncovers a link between glycolysis, mitochondrial physiology, and tumor maintenance. *Cancer Cell.* 2006;9:425–434.
32. Medina MA, Sanchez-Jimenez F, Marquez J, et al. Relevance of glutamine metabolism to tumor cell growth. *Mol Cell Biochem.* 1992;113:1–15.
33. Moreadith RW, Lehninger AL. The pathways of glutamate and glutamine oxidation by tumor cell mitochondria. Role of mitochondrial NAD(P)+-dependent malic enzyme. *J Biol Chem.* 1984;259:6215–6221.
34. Cairns RA, Harris IS, Mak TW. Regulation of cancer cell metabolism. *Nat Rev Cancer.* 2011;11:85–95.
35. Yao X, Zeng M, Wang H, et al. Metabolite detection of pancreatic carcinoma by in vivo proton MRspectroscopy at 3T: initial results. *Radiol Med.* 2012;117:780–788.
36. Sandgren EP, Quaife CJ, Paulovich AG, et al. Pancreatic tumor pathogenesis reflects the causative genetic lesion. *Proc Natl Acad Sci U S A.* 1991;88:93–97.
37. Hong SM, Park JY, Hruban RH, et al. Molecular signatures of pancreatic cancer. *Arch Pathol Lab Med.* 2011;135:716–727.
38. Shim H, Dolde C, Lewis BC, et al. c-*myc* transactivation of LDH-A: implications for tumor metabolism and growth. *Proc Natl Acad Sci U S A.* 1997;94:6658–6663.
39. Yamamura S, Saini S, Majid S, et al. MicroRNA-34a modulates c-*myc* transcriptional complexes to suppress malignancy in human prostate cancer cells. *PLoS One.* 2012;7:e29722.
40. Hermeking H. The miR-34 family in cancer and apoptosis. *Cell Death Differ.* 2010;17:193–199.
41. Sotillo E, Laver T, Mellert H, et al. *Myc* overexpression brings out unexpected antiapoptotic effects of miR-34a. *Oncogene.* 2011;30:2587–2594.
42. Dhayat S, Mardin WA, Mees ST, et al. Epigenetic markers for chemosensitivity and chemoresistance in pancreatic cancer—a review. *Int J Cancer.* 2011;129:1031–1041.
43. Arlt A, Gehrz A, Muerkoster S, et al. Role of NF-kappaB and Akt/PI3K in the resistance of pancreatic carcinoma cell lines against gemcitabine-induced cell death. *Oncogene.* 2003;22:3243–3251.
44. Kawauchi K, Araki K, Tobiume K, et al. p53 regulates glucose metabolism through an IKK-NF-kappaB pathway and inhibits cell transformation. *Nat Cell Biol.* 2008;10:611–618.
45. Hirayama A, Kami K, Sugimoto M, et al. Quantitative metabolome profiling of colon and stomach cancer microenvironment by capillary electrophoresis time-of-flight mass spectrometry. *Cancer Res.* 2009;69:4918–4925.
46. Phang JM, Donald SP, Pandhare J, et al. The metabolism of proline, a stress substrate, modulates carcinogenic pathways. *Amino Acids.* 2008;35:681–690.
47. Liu Y, Borchert GL, Donald SP, et al. Proline oxidase functions as a mitochondrial tumor suppressor in human cancers. *Cancer Res.* 2009;69:6414–6422.
48. Maehara S, Tanaka S, Shimada M, et al. Selenoprotein P, as a predictor for evaluating gemcitabine resistance in human pancreatic cancer cells. *Int J Cancer.* 2004;112:184–189.
49. Wheatley DN. Arginine deprivation and metabolomics: important aspects of intermediary metabolism in relation to the differential sensitivity of normal and tumour cells. *Semin Cancer Biol.* 2005;15:247–253.
50. Crabtree MJ, Channon KM. Synthesis and recycling of tetrahydrobiopterin in endothelial function and vascular disease. *Nitric Oxide.* 2011;25:81–88.
51. Fujita H, Ohuchida K, Mizumoto K, et al. Gene expression levels as predictive markers of outcome in pancreatic cancer after gemcitabine-based adjuvant chemotherapy. *Neoplasia.* 2010;12:807–817.
52. Kolberg M, Strand KR, Graff P, et al. Structure, function, and mechanism of ribonucleotide reductases. *Biochim Biophys Acta.* 2004;1699:1–34.
53. Hatse S, De Clercq E, Balzarini J. Role of antimetabolites of purine and pyrimidine nucleotide metabolism in tumor cell differentiation. *Biochem Pharmacol.* 1999;58:539–555.

Journal of Virological Methods 201 (2014) 20–23

Contents lists available at ScienceDirect

Journal of Virological Methods

journal homepage: www.elsevier.com/locate/jviromet

Short communication

Liver cell-specific peptides derived from the preS1 domain of human hepatitis B virus

Jeong-Hun Kang[a,*], Riki Toita[b], Daisuke Asai[c], Tetsuji Yamaoka[a], Masaharu Murata[d]

[a] Department of Biomedical Engineering, National Cerebral and Cardiovascular Center Research Institute, 5-7-1 Fujishirodai, Suita, Osaka 565-8565, Japan
[b] Department of Biomaterials, Faculty of Dental Science, Kyushu University, 3-1-1 Maidashi, Higashi-ku, Fukuoka-shi, Fukuoka 812-8582, Japan
[c] Department of Microbiology, St. Marianna University School of Medicine, Sugao 2-16-1, Miyamae, Kawasaki, Kanagawa 216-8511, Japan
[d] Department of Advanced Medical Initiatives, Faculty of Medical Sciences, Kyushu University, 3-1-1 Maidashi, Higashi-ku, Fukuoka 812-8582, Japan

Article history:
Received 30 September 2013
Received in revised form 7 February 2014
Accepted 11 February 2014
Available online 22 February 2014

Keywords:
Human hepatitis B virus
preS1
Hepatocellular carcinoma
Hepatocyte
Peptide substrate

A B S T R A C T

The envelope of human hepatitis B virus (HBV) consists of the large (L), middle (M), and small (S) surface proteins. The preS1 domain at the N terminus of the L-protein is essential for recognizing a target cell and for viral infectivity. In the present study, peptides derived from the preS1 domain (amino acid residues 2–19) were synthesized, and their binding affinities for human hepatocellular carcinoma (HCC) cells were determined. Non-myristoylated peptides showed much lower affinity for HepG2 cells than myristoylated peptides. Although all peptides showed significantly higher affinities for two human HCC cell lines (HepG2 and HuH-7) compared with other cell lines (HeLa, B16, NMuLi, and NIH 3T3), a modified peptide exhibited the highest affinity for HCC cell lines. These results suggest that the modified peptide can target liver cells.

The human hepatitis B virus (HBV) is a small enveloped DNA virus that causes acute and chronic infections of the liver. The HBV envelope consists of the large (L), middle (M), and small (S) surface proteins. L- and M-proteins contain the S-protein [226 amino acid (aa) residues] and 55 hydrophilic aa residues at the N terminus of the S-protein (preS2), and the L-protein has an extension of hydrophilic residues (108 or 119 depending on genotype) (called preS1) at the N terminus of preS2 (Glebe and Urban, 2007; Meier et al., 2013; Seeger and Mason, 2000).

preS1 is essential for virus infection, but not preS2. preS1 is myristoylated at glycine residue in position 2 and myristoylation increases viral infectivity (Glebe et al., 2005; Glebe and Urban, 2007; Meier et al., 2013; Seeger and Mason, 2000). Further, the preS1 domain has a receptor binding site containing essential aa residues 9–18 and recognizes the asialoglycoprotein receptor on the surface of human hepatocytes or hepatocellular carcinoma (HCC) cells (Engelke et al., 2006; Glebe et al., 2005; Zhang et al., 2011).

In the present study, preS1-derived peptides were synthesized, and their binding specificity for human HCC cells was examined using two human HCC cell lines (HepG2 and HuH-7), the human epithelial carcinoma HeLa cell line, the mouse melanoma B16 cell line, the normal mouse liver epithelial NMuLi cell line, and the mouse embryo fibroblast NIH 3T3 cell line.

Fluorescent peptides labeled with FITC with or without myristic acid were synthesized by Scrum Inc. (Tokyo, Japan). The purities of the synthetic peptides were determined using high-performance liquid chromatography and matrix-assisted laser desorption/ionization-time-of-flight mass spectrometry. Peptides with purities >95% were used (Table S1 and Fig. S1).

All cell lines were maintained in Dulbecco's Modified Eagle's Medium (Gibco, Invitrogen Co., Grand Island, NY, USA). Media were supplemented with 10% FBS, penicillin (100 U/mL), streptomycin (100 μg/mL), and amphotericin B (0.25 μg/mL) (all from Gibco). The cells were incubated at 37 °C in a humidified atmosphere containing 5% CO_2.

To determine the affinity of peptides for each cell line, cells (5×10^5) were grown in 6-well plates at 37 °C for 24 h. After 24 h peptides (5 μM) were added to each plate and were incubated for 24 h. Micrographs of the cells were obtained using fluorescence microscopy, and images were analyzed using AQUACOSMOS 2.6

* Corresponding author. Tel.: +81 6 6833 5012; fax: +81 6 6835 5476.
E-mail address: jrjhkang@ncvc.go.jp (J.-H. Kang).

http://dx.doi.org/10.1016/j.jviromet.2014.02.013
0166-0934/

A

Genotypes	Sequences
A	GTNLSVPNPLGFFPDHQL
B	GTNLSVPNPLGFFPDHQL
C	GTNLSVPNPLGFFPDHQL
D	GQNLSTSNPLGFFPDHQL
E	GKNISTTNPLGFFPDHQL
F	GQNLSVPNPLGFFPDHQL
G	GKNLSASNPLGFLPDHQL
H	GQNLSVPNPLGFFPDHQL

B

Samples	Sequences
HBV-11-1	GTNLSVPNPLGFFPDHQL
HBV-11-2	GQNLSTSNPLGFFPDHQL
HBV-11-3	GQNLSVSNPLGFFPEHQL

Fig. 1. (A) Comparison of aa residues 2–19 from the preS1 domain of HBV genotypes (A–H). These sequences contain a region (aa residues 9–18) that is essential for binding to the surface receptor of human hepatocytes or HCC cells. (B) Peptide sequences. HBV-11-1 and HBV-11-2 were derived from preS1 of HBV genotypes A, B, and C as well as HBV genotype D, respectively, and HBV-11-3 was obtained by modification of the preS1 peptide.

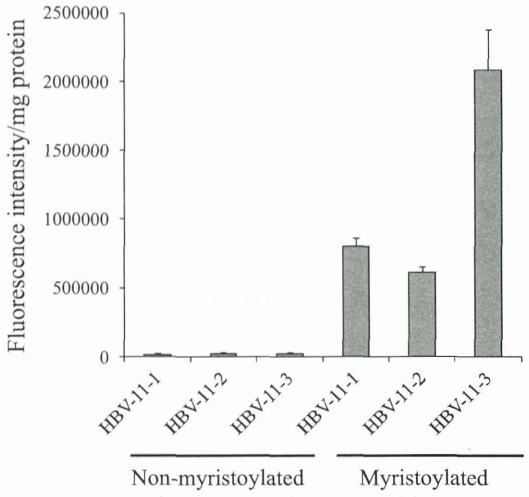

Fig. 2. Binding affinity of myristoylated or non-myristoylated peptides for HepG2 cells. The fluorescence intensities are presented as fluorescence intensity/mg total protein.

software (Hamamatsu Photonics, Shizuoka, Japan). To determine fluorescence intensity, each well was washed three times with phosphate-buffered saline, and cells were scraped off the surface of the well and lysed in 500 μL of lysis buffer (100 mM Tris–HCl, pH 7.2, 1% Triton-X 100, and 2 mM EDTA). Fluorescence intensity was detected using a Wallac ARVO SX 1420 multilabel counter (Perkin-Elmer Life Science, Japan, Co. Ltd., Kanagawa, Japan). Total protein concentration was determined using the Bradford method (Coomassie Brilliant Blue G-250 reagent; Bio-Rad Lab., Hercules, CA, USA), and absorbance was determined at 595 nm.

Results are expressed as fluorescence intensity/mg total protein and as the mean and standard deviation of six samples. All determinations were performed in duplicate. Statistical analysis of the differences between means was performed using Student's *t* test.

Synthetic peptides used in this study were derived from the N-terminal region of the preS1 domain (aa residues 2–19) (Fig. 1A). These regions contain essential receptor and host cell binding sites, but not epitopes recognized by the immune system (Bremer et al., 2011; Glebe and Urban, 2007; Hu et al., 2005). There are eight HBV genotypes (A–H), and their geographical distributions differ (Mahtab et al., 2008; McMahon, 2009). The HBV-11-1 peptide is derived from the preS1 of HBV genotypes A, B, and C, and HBV-11-2 is derived from HBV genotype D. The HBV-11-3 peptide was obtained by a modification of native preS1 peptide sequences. In particular, the aspartate (D) residue at position 16 was replaced with a glutamate (E). The side chain of a glutamate residue is longer and is slightly more flexible than that of an aspartate residue, but chains are functionally similar (Fig. 1B).

To determine whether myristoylation of the glycine residue at position 2 influences the affinity of the peptide for binding to human HCC HepG2 cells, peptides with or without myristic acid were synthesized and added to HepG2 cells. Non-myristoylated peptides bound with much lower affinity to HepG2 cells compared with myristoylated peptides (Fig. 2).

Further, the cell binding specificities of the peptides were determined using six cell lines. Higher fluorescence levels ($P < 0.01$) were observed for two human HCC cell lines (HepG2 and HuH-7) compared with cell lines (HeLa, B16, NMuLi, and NIH 3T3) (Fig. 3 and Fig. S2). Interestingly, the modified peptide HBV-11-3 showed significantly higher fluorescence levels ($P < 0.001$) for HepG2 and HuH-7 cells compared with the two unmodified peptides (HBV-11-1 and HBV-11-2) (Fig. 3).

Natural and synthetic compounds that specifically target liver cells are very useful for treating liver diseases such as HCC, hepatitis B and C, as well as metabolic disease caused by liver dysfunction. Several studies show that preS1 effectively targets human hepatocytes or HCC cells, and preS1-conjugated carriers efficiently deliver genes or drugs into human hepatocytes or HCC cells (Kang et al., 2010; Lee et al., 2012; Miyata et al., 2009; Murata et al., 2012). For example, an HCC-targeted gene delivery system prepared by incorporating a tumor cell-specific gene regulation system into bio-nanocapsules containing preS1 increased transfection efficiency and selectivity for human HCC cells, but gene expression was not detected in normal human hepatocytes and other tumor cell lines (human epidermoid carcinoma A431 cells and human lung adenocarcinoma A549 cells) (Kang et al., 2010). Further, preS1-derived peptides inhibit attachment and infection of HBV to its target cells (Engelke et al., 2006; Glebe et al., 2005; Gripon et al., 2005).

Despite these advantages, use of intact preS1 may induce an immune response. To address these issues, the myristoylated peptides derived from the preS1 domain (regions 2–19) were synthesized, and their affinities for HCC cells were determined. Although HBV-11-1 and HBV-11-2 showed significantly higher affinities for HepG2 and HuH-7 cells compared with other cell lines (HeLa, B16, NMuLi, and NIH 3T3), HBV-11-3 exhibited the highest affinity for HCC cell lines.

In conclusion, myristoylated peptides derived from amino acid residues 2–19 of the preS1 domain selectively recognized human HCC cell lines, and HBV-11-3 peptides bound with the highest affinities to human HCC cell lines.